ARTICLE

Bi-allelic Pathogenic Variants in *HS2ST1* Cause a Syndrome Characterized by Developmental Delay and Corpus Callosum, Skeletal, and Renal Abnormalities

Pauline E. Schneeberger,[1,7] Leonie von Elsner,[1,7] Emma L. Barker,[2] Peter Meinecke,[1] Iris Marquardt,[3] Malik Alawi,[4] Katharina Steindl,[5] Pascal Joset,[5] Anita Rauch,[5] Petra J.G. Zwijnenburg,[6] Marjan M. Weiss,[6] Catherine L.R. Merry,[2] and Kerstin Kutsche[1,*]

Summary

Heparan sulfate belongs to the group of glycosaminoglycans (GAGs), highly sulfated linear polysaccharides. Heparan sulfate 2-*O*-sulfotransferase 1 (HS2ST1) is one of several specialized enzymes required for heparan sulfate synthesis and catalyzes the transfer of the sulfate groups to the sugar moiety of heparan sulfate. We report bi-allelic pathogenic variants in *HS2ST1* in four individuals from three unrelated families. Affected individuals showed facial dysmorphism with coarse face, upslanted palpebral fissures, broad nasal tip, and wide mouth, developmental delay and/or intellectual disability, corpus callosum agenesis or hypoplasia, flexion contractures, brachydactyly of hands and feet with broad fingertips and toes, and uni- or bilateral renal agenesis in three individuals. *HS2ST1* variants cause a reduction in *HS2ST1* mRNA and decreased or absent heparan sulfate 2-*O*-sulfotransferase 1 in two of three fibroblast cell lines derived from affected individuals. The heparan sulfate synthesized by the individual 1 cell line lacks 2-*O*-sulfated domains but had an increase in *N*- and 6-*O*-sulfated domains demonstrating functional impairment of the HS2ST1. As heparan sulfate modulates FGF-mediated signaling, we found a significantly decreased activation of the MAP kinases ERK1/2 in FGF-2-stimulated cell lines of affected individuals that could be restored by addition of heparin, a GAG similar to heparan sulfate. Focal adhesions in FGF-2-stimulated fibroblasts of affected individuals concentrated at the cell periphery. Our data demonstrate that a heparan sulfate synthesis deficit causes a recognizable syndrome and emphasize a role for 2-*O*-sulfated heparan sulfate in human neuronal, skeletal, and renal development.

Introduction

Heparan sulfate proteoglycans (HSPGs) are glycoproteins composed of a core protein to which heparan sulfate (HS), a highly sulfated linear polysaccharide (glycosaminoglycan; GAG), is attached. HSPGs are either associated with the plasma membrane or excreted into the extracellular matrix.[1,2] *In vitro* and *in vivo* studies have demonstrated the important role of HSPGs in various signaling pathways during development. In particular, HS binds to several secreted signaling molecules, such as members of the Wnt/wingless, Hedgehog, transforming growth factor-beta, and fibroblast growth factor (FGF) families.[2–4] These signaling molecules typically require the presence of HS for high-affinity interactions with tyrosine kinase receptors, with structural modifications within the polysaccharide, e.g., 2-*O*-sulfation, of particular importance for selective triggering of specific transduction pathways, such as FGF-mediated signaling.[5–7]

The complex biosynthesis of HS takes place, and is controlled, in the Golgi apparatus and requires the interdependent activity of a family of specialized enzymes.[1] One of the transferases and modifying enzymes responsible for HS synthesis is heparan sulfate 2-*O*-sulfotransferase 1 (HS2ST1) that catalyzes the transfer of the sulfate group from 3′-phosphoadenosine 5′-phosphosulfate (PAPS) to the 2-OH position of two uronic acids, glucuronic acid (GlcA) and iduronic acid (IdoA).[8,9] As HS2ST1 preferentially acts on IdoA over GlcA, IdoA residues are commonly 2-*O*-sulfated in HS. All HS species analyzed to date are substantially 2-*O*-sulfated and have sulfated domains rich in 2-*O*-, 6-*O*-, and *N*-sulfated residues. 2-*O*-sulfated GlcA units are rarely present.[10,11] In most vertebrate genomes, only one gene encoding an HS2ST isoform exists. The enzymes share a high sequence homology across species, with 75% similarity of human HS2ST1 to insect and 67% to *Caenorhabditis elegans* Hs2st1, suggesting a crucial physiological role in these organisms.[12,13] While *Drosophila Hs2st* mutants survive to the adult stage without obvious morphological defects,[14] *C. elegans* Hs2st mutants display defects in cell migration and nervous system development, particularly axon patterning.[15,16] A more severe phenotype was observed in mice homozygous for a gene trap mutation in *Hs2st1*. Knockout mice are stillborn or die within the first day of life. All mutant mice show bilateral renal agenesis and eye and skeletal abnormalities.[17] Together,

[1]Institute of Human Genetics, University Medical Center Hamburg-Eppendorf, 20246 Hamburg, Germany; [2]Nottingham Biodiscovery Institute, University of Nottingham, University Park NG7 2RD, UK; [3]Klinik für Neuropädiatrie und angeborene Stoffwechselerkrankungen, Klinikum Oldenburg, 26133 Oldenburg, Germany; [4]Bioinformatics Core, University Medical Center Hamburg-Eppendorf, 20246 Hamburg, Germany; [5]Institute of Medical Genetics, University of Zürich, 8952 Schlieren, Switzerland; [6]Department of Clinical Genetics, Amsterdam University Medical Center, 1081 Amsterdam, the Netherlands
[7]These authors contributed equally to this work
*Correspondence: kkutsche@uke.de
https://doi.org/10.1016/j.ajhg.2020.10.007.

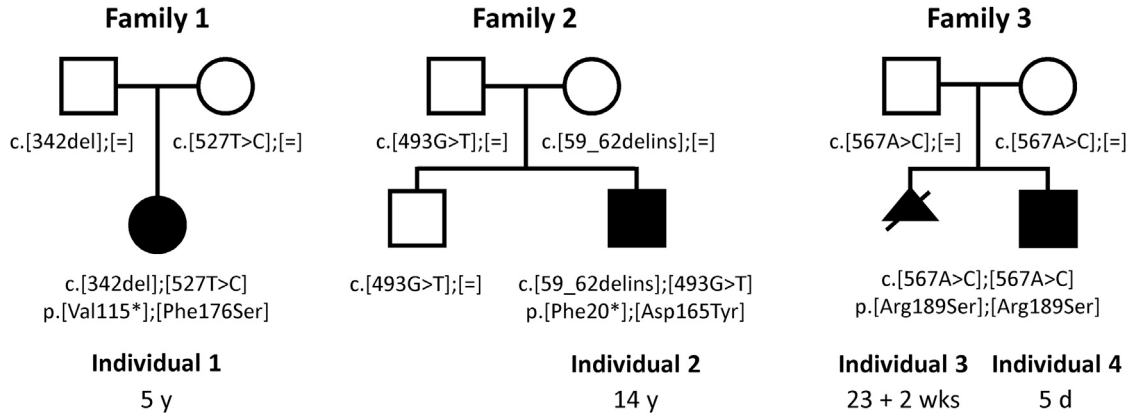

Figure 1. Pedigree of Individuals with Bi-allelic Variants in *HS2ST1*
Age at last examination and identified variants in *HS2ST1* in the four affected individuals and members of three families are given below each pedigree. For individual 3, the gestational age at induced termination of pregnancy is given. d, days; wks, weeks; y, years.

data from animal studies indicate that 2-*O*-sulfated HS is required for morphogenesis during vertebrate development.[18]

The molecular consequences of *Hs2st1* deficiency on the structural and functional properties of HS have been studied in primary mouse embryonic fibroblasts. In these cells, the biosynthetic machinery produces a novel HS structure lacking 2-*O*-sulfate groups but maintaining the overall charge density with increases in *N*- and 6-*O*-sulfation.[19] Compositional HS disaccharide profiling in *Drosophila Hs2st* mutants has demonstrated a similar compensatory mechanism suggesting that the retention of charge level and distribution in HS may be responsible for the mild phenotype of the *Hs2st* mutants, with 6-*O*-sulfate groups replacing 2-*O*-sulfate groups during *Drosophila* development.[14] In contrast, the structurally altered HS generated in *Hs2st1* knockout mice is able to compensate for the function of the wild-type chains in many but not all tissues during development.[19]

Here we report bi-allelic *HS2ST1* variants in four affected individuals from three unrelated families. The core phenotype in these individuals, including one severely affected fetus, comprises developmental delay and/or intellectual disability in the three live individuals, and corpus callosum agenesis or hypoplasia, facial dysmorphism, short stature, and other skeletal abnormalities. Uni- or bilateral renal agenesis was present in three of the four affected individuals. For *in vitro* studies, we used fibroblasts of three unrelated affected individuals and found decreased or no HS2ST1 protein in two cell lines, lack of 2-*O*-sulfated HS in individual 1 cells, low FGF-2-induced activation of the MAP kinases ERK1/2 that can be restored by exogeneous addition of the GAG heparin, and altered location of focal adhesions in fibroblasts from affected individuals. Our data suggest that strongly diminished or absent HS 2-*O*-sulfotransferase 1 activity underlies the syndromic clinical presentation in the four individuals reported here.

Subjects and Methods

Study Approval

Informed consent for genetic analyses was obtained for all affected individuals, and genetic studies were performed clinically or as approved by the Institutional Review Boards of the relevant institutions. The parents of the affected individuals provided written informed consent for participation in the study, clinical data and specimen collection, genetic analysis, and publication of relevant findings. Permission to publish photographs and radiographs was provided for individuals shown in Figures 2 and 3.

Whole-Exome Sequencing, Sequence Data Analysis, and Variant Validation

Individual 1

Whole-exome sequencing (WES) was performed on genomic DNA extracted from leukocytes of individual 1 and her healthy parents by CeGaT. Enrichment was carried out using the SureSelect Human All Exon V6 kit (Agilent). Each captured library was loaded and sequenced on the HiSeq platform (Illumina). Sequence reads were aligned to the human reference assembly (UCSC hg19) using the Burrows Wheeler Aligner (BWA mem, v.0.7.17-r1188).[20] Variant discovery was performed with the Genome Analysis Toolkit (GATK, v.3.8),[21] following the best practice recommendations of the developers. Afterward, variants were functionally annotated and compared to those documented in publicly accessible genetic variant databases (e.g., dbSNP138, ClinVar, ExAC, and gnomAD) using AnnoVar (v.2018-04-16).[22] Only exonic and intronic variants that were private (absent in public database), rare (with a minor allele frequency [MAF] of $\leq$ 0.1% and no homozygotes in public databases), or located at exon-intron boundaries ranging from −10 to +10 were retained. These variants should be absent (*de novo* in individual 1) or present in the heterozygous state in the healthy parents (homozygous or compound heterozygous in individual 1). Exonic and splice variants were then prioritized by pathogenicity assessment using multiple *in silico* tools (CADD, REVEL, M-CAP, Human Splicing Finder 3.1, NetGene2-Server, and Berkeley *Drosophila* Genome Project-Database).

Sequence validation and segregation analysis of the *HS2ST1* variants c.342delA (p.Val115*) and c.527T>C (p.Phe176Ser)

Figure 2. Photographs of Individuals with Bi-allelic *HS2ST1* Variants

(A and B) Face of individual 1 at age 3.5 years. Note prominent forehead with bitemporal narrowing, thick eyebrows, hypertelorism, upslanted and asymmetry of palpebral fissures, bilateral epicanthus, broad nasal root and tip, and wide mouth.

(C) Hands of individual 1 at age 5 years showing brachydactyly with broad and bulbous fingertips.

(D and E) Feet of individual 1 at age 5 years with plantar malposition of 4th toes and short toes with bulbous tips.

(F and G) Face of individual 2 at age 10 years. He had coarse face with upslanted palpebral fissures, broad nasal tip, wide mouth, full lips, deep philtrum, and small teeth.

(H and I) Feet and left hand of individual 2 at age 12 years. Note broad thumb and toes, bilateral pes planovalgus, and camptodactyly of 2nd to 5th toes on the right and of the 5th toe on the left.

(J) Individual 3 (fetus) had flexion contractures of elbows and knees, supination of both feet, and brachydactyly with broad thumbs and halluces.

(K) Coarse facial appearance of individual 4 as newborn. He had short and upslanted palpebral fissures, broad nasal root, bridge and nasal tip, long and deep philtrum, wide mouth, thin upper lip vermilion, everted lower lip vermilion, pointed chin with retrognathia, and full and sunken cheeks.

(L and M) Hands and feet of individual 4 show brachydactyly with broad and bulbous fingertips and toes.

(GenBank: NM_012262.4) was performed on leukocyte-derived DNA from individual 1 and parents and also on fibroblast-derived DNA and cDNA from individual 1 by Sanger sequencing. Primer sequences are described in Table S1.

Individual 2

WES was performed on genomic DNA extracted from leukocytes of individual 2 and his healthy parents. 2.5 mg of DNA was sheared on a Covaris S2 instrument (Covaris). DNA libraries were prepared using Kapa Biosystems reagents, and 1.0 mg of the library was used for enrichment with Roche/NimbleGen SeqCap EZ MedExome (Roche) according to the manufacturer's protocol. Sequencing was performed on an Illumina HiSeq 2500 platform (Illumina) with 125 bp paired-end reads. More than 91% of the capture region was covered $\geq$ 30× with a mean bait coverage of approximately 100× for each sample. Variant calling was performed using an in-house analysis pipeline. Alignment of sequence reads to the human genome (hg19) was performed with the Burrows–Wheeler Aligner tool (BWA-MEM v0.7.10) using default settings. Picard Tools (v1.111) was used for sorting and marking duplicates. For local realignment and base quality score recalibration, we used the Genome Analysis Toolkit (GATK; v.3.3-0), and for variant calling, we used the GATK HaplotypeCaller. Variants were filter tagged using the GATK VariantFiltration and annotated by snpEff (v.4.0). Variant prioritization was performed using Cartagenia Bench Lab NGS (Agilent Technologies). In short, a classification tree was used to select for variants present in individual 2 with MAF < 1% in control cohorts (dbSNP build 142), 1000 Genomes Phase 3 release v.5.20130502, and ESP6500 as well as in-house controls. Prerequisite was that these variants had been genotyped in at least 200 alleles. Subsequently, the remaining variants were further prioritized based on literature, predicted (deleterious) effects on protein function by, e.g., truncating the protein, affecting splicing, amino acid change, and evolutionary conservation. The two identified *HS2ST1* variants were genotyped in DNA of individual 2's healthy brother by Sanger sequencing.

Individuals 3 and 4

Genomic DNA was extracted from amniotic fluid (individual 3), cultivated fibroblast cells (individual 4), and EDTA blood samples from the parents. Trio WES in individual 3 and parents was performed using the IDT Kit (v1.0) with paired-end sequencing (NovaSeq 6000 S1 Reagent Kit (300 cycles), 150

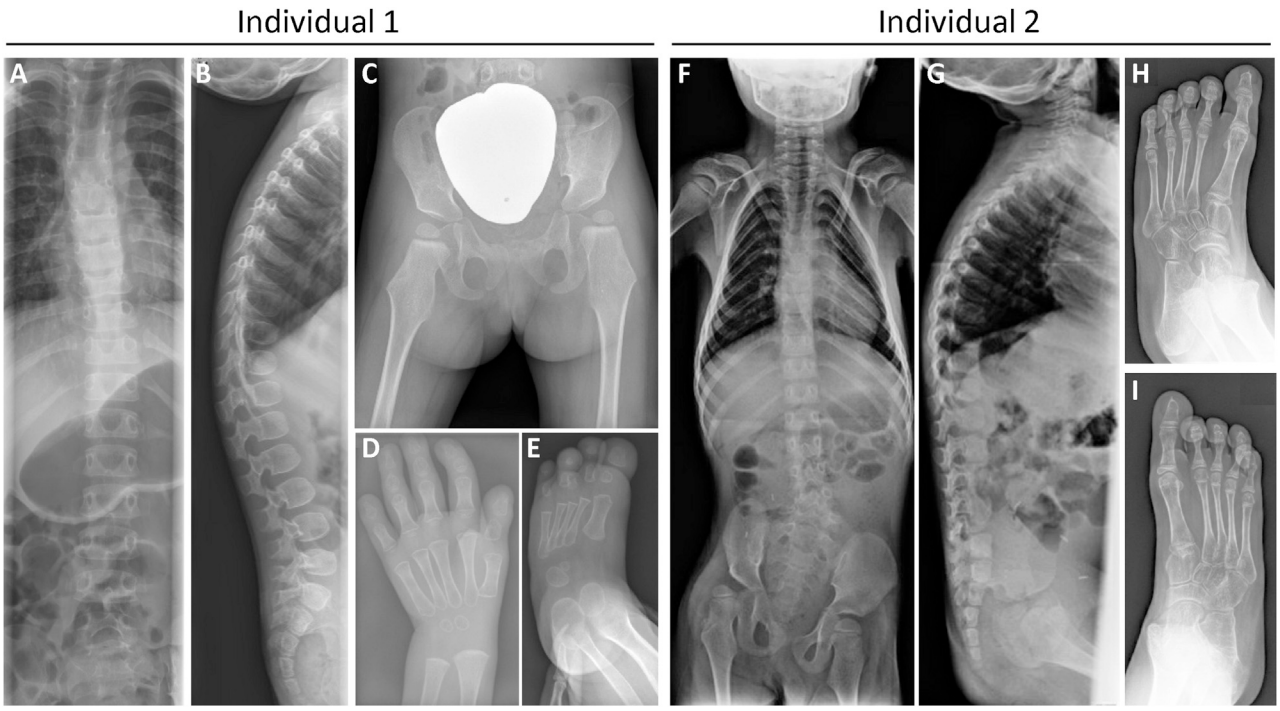

Figure 3. Radiographic Images of Individuals 1 and 2 with Bi-allelic *HS2ST1* Variants
(A and B) Spine radiograph of individual 1 at age 2 years, 3 months. Anterior-posterior view showed thoracic scoliosis. Lateral view revealed marked kyphosis of the thoracic spine with bi-convex, "barrel-shaped" vertebral bodies and narrowing of lumbar spinal canal.
(C) Pelvis radiograph at age 2 years, 3 months: narrow iliac bones, subluxation of the left femoral head, coxa valga, and maturation delay of proximal femoral epiphyses.
(D) X-ray of left hand at age 3.5 years: bone maturation was markedly delayed with two carpals only and lack of radial epiphysis, brachydactyly of all phalanges with particularly short and ovoid middle 2nd to 5th phalanges, lack of the 5th middle phalanx, and short 1st proximal phalanx.
(E) X-ray of left foot at age 15 months: bone maturation was delayed, proximal phalanges were short and poorly modeled, and middle phalanges showed reduced ossification.
(F and G) Spine radiographs of individual 2 at age 6 years demonstrate kyphosis of the thoracic spine and scoliosis of the lower lumbar spine to the left due to hemivertebra L5.
(H and I) X-rays of feet at age 12 years show flexion contractures of 2nd to 5th toes.

Fwd-150 Rev, Q30-Wert: 92.6%) on a NovaSeq System (Illumina). Raw fastQ files were aligned to the hg19 reference genome using the NextGENe software v.2.4.2.3 (SoftGenetics). The average depth of coverage was 285×, and about 99.4% of the targeted bases were covered by ≥ 20 sequence reads. Coding plus intronic (±6 bp) variants observed in at least 16% of reads with sufficient quality level and with MAF ≤ 2% were investigated using the NextGENe Software (SoftGenetics) for (1) *de novo* non-synonymous variants, (2) homozygous/hemizygous non-synonymous variants, (3) compound heterozygous non-synonymous variants, and (4) synonymous variants within 3 bp away from exon-intron-boundaries potentially affecting splicing. Candidate variants were further investigated for deleterious effects by various *in silico* tools, the presence or absence in relevant genetic databases (ClinVar, HGMD, gnomAD, CADD), by association of the gene with the proband's phenotype, by literature search for evident functional information, and by GeneMatcher entry for matching with unrelated, similarly affected subjects. The *HS2ST1* variant c.567A>C (p.Arg189Ser) was confirmed to be present in individuals 3 and 4 in the homozygous state by Sanger sequencing using an ABI Genetic Analyzer 3730 (Applied Biosystems).

Transcript Analysis

RNA isolation, complementary DNA (cDNA) synthesis, and quantitative reverse transcription PCR (RT-qPCR) to determine the relative *HS2ST1* mRNA amount in fibroblasts of affected and healthy individuals were performed as previously described.[23] Qualitative RT-PCR to analyze *HS2ST1* transcripts was performed on fibroblast-derived cDNA according to standard PCR protocols with the OneTaq Quick-Load 2X Master Mix (New England Biolabs). PCR products were directly Sanger-sequenced. Primer sequences are described in Table S1.

Antibodies

The following primary antibodies and dilutions were used: mouse monoclonal anti-HS2ST1 (1:500; Santa Cruz Biotechnology; sc-376530; clone G-10); rabbit polyclonal anti-p44/42 MAPK (ERK1/2) (1:1,000; Cell Signaling Technology [CST]; #9102); rabbit polyclonal anti-phospho-p44/42 MAPK (ERK1/2) (Thr202/Tyr204) (1:1,000; CST; #9101); and mouse monoclonal anti-paxillin (IF: 1:100, WB: 1:1,000; BD Transduction Laboratories; #612405; clone 349).

The following secondary antibodies and dilutions were used: goat anti-mouse IgG:StarBright Blue 700 antibody (1:5,000 or 1:10,000; BioRad; #12004159); hFAB Rhodamine anti-GAPDH

IgG (1:5,000; BioRad; #12004167); hFAB Rhodamine anti-Tubulin IgG (1:5,000; BioRad; #12004165); goat anti-mouse Alexa Fluor 488-conjugated secondary antibody (1:1,000; Invitrogen; #A11029).

Cell Culture

Primary fibroblasts obtained from a skin biopsy from individuals 1, 2, and 3 and four healthy individuals (control subjects) were cultured in Dulbecco's modified Eagle medium (DMEM; Thermo Fisher Scientific) supplemented with 10% fetal bovine serum (FBS; GE Healthcare) and penicillin-streptomycin (100 U/mL and 100 μg/mL, respectively; Thermo Fisher Scientific). Cells were tested for mycoplasma contamination by PCR and confirmed to be mycoplasma free.

Immunoblot Analysis

Cell lysates from affected individuals' and control fibroblasts were prepared, and immunoblotting was performed as previously described.[23] Briefly, cells were harvested in ice-cold RIPA buffer and protein extracts were separated on SDS-PAGE and transferred to polyvinylidene fluoride membranes. The membrane was incubated with the indicated primary antibody at 4°C overnight and fluorescent dye-linked secondary antibodies at room temperature for 1 h.

ERK Phosphorylation

Fibroblasts were seeded into 6-well plates (150,000 cells per well) and incubated in starvation medium (0.1% FBS/DMEM) overnight. The next day, cells were treated with 10 ng/mL recombinant human FGF-2 (R&D Systems) in starvation medium for either 10 min or 20 min or left untreated. For the rescue experiment, cells were treated with 10 ng/mL FGF-2 and 30 ng/mL heparin sodium salt from porcine intestinal mucosa (Sigma-Aldrich), and for control purposes cells were solely treated with 30 ng/mL heparin sodium salt. Subsequently, plates were transferred on ice and rinsed with ice-cold PBS. Cells were harvested in ice-cold RIPA buffer supplemented with Mini Protease Inhibitor and PhosSTOP (Roche), and lysates were subjected to SDS-PAGE and immunoblot analysis. For quantification, pERK1/2 was normalized to total ERK1/2, and the ratio at 0 min was set to 1.

Disaccharide Analysis

Cultured primary fibroblasts from individual 1 and two healthy individuals were seeded in T75 flasks. After 3–4 days, cells were washed with PBS, then lysed using 1% (vol/vol) Triton X-100/PBS for 30 min at room temperature while shaking. Conditioned-media and cell extract samples were treated with 100 mg/mL Pronase (Roche Diagnostics) for 4 h at 37°C. Cell extracts were incubated for 15 min at 90°C to deactivate the Pronase, before treating with 14 mg/mL DNase I (Sigma-Aldrich) and 10 mM $MgCl_2$ overnight at 37°C to prevent DNA interference with downstream processing. All preparations were loaded onto 1 mL diethylaminoethyl (DEAE)-Sephacel columns (Sigma-Aldrich) and washed with 50 mL of 0.25 M NaCl, 20 mM $NaH_2PO_4.H_2O$ (pH 7.0) to remove hyaluronan. The sulfated GAGs were eluted with 5 mL of 1.5 M NaCl, 20 mM $NaH_2PO_4.H_2O$ (pH 7.0) and desalted using PD-10 Sephadex G-25M pre-packed columns (GE Healthcare). Purified GAGs were freeze-dried, then digested using 0.8 mIU of each heparinase I, II, and III (from *Flavobacterium heparinum*, Iduron) in 100 mL of 0.1 M sodium acetate and 0.1 mM calcium acetate (pH 7.0) for 12 h at room temperature. The resulting disaccharides were freeze-dried, then re-suspended in 10 mL of 0.1 M 2-aminoacridone (AMAC) and incubated at room temperature for 20 min. To each reaction, 10 mL of 1M $NaBH_3CN$ was added, and incubation continued at room temperature overnight in the dark. The AMAC-labeled samples were separated by RP-HPLC in duplicate using a Zorbax Eclipse XDB-C18 RP-HPLC column (35 mM, 2.1 mm × 150 mm; Agilent Technologies), as described previously.[24,25] Disaccharides were detected by fluorescence and were identified and quantified in comparison with known amounts of commercial disaccharide standards (Iduron). As described previously, due to the efficiency of AMAC labeling varying according to specific disaccharides, the raw peaks were multiplied by predetermined correction factors.[24]

Immunocytochemistry

50,000 cells per well were seeded on coverslips in 12-well plates and incubated in starvation medium (0.1% FBS/DMEM) overnight. The next day, cells were incubated with 10 ng/mL FGF-2 in starvation medium for 1 h. Subsequently, cells were rinsed with PBS, fixed with 4% paraformaldehyde (Morphisto) in PBS, and washed three times with PBS. After treatment with permeabilization/blocking solution (2% BSA, 3% goat serum, 0.5% Nonidet P40 in PBS), cells were incubated in antibody solution (3% goat serum and 0.1% Nonidet P40 in PBS) containing mouse anti-paxillin primary antibody. Cells were washed with PBS and incubated with Alexa Fluor 488-conjugated anti-mouse secondary antibody in antibody solution. After extensive washing with PBS, cells were embedded in ProLong Diamond Antifade Mountant with DAPI (Invitrogen) on microscopic slides. Cells were imaged with a widefield Zeiss fluorescence microscope system (Zeiss Axiovert 200M) equipped with a 63× oil immersion objective lens and an Apotome unit. Images of representative cells were taken to visualize and quantify the observed morphological changes.

Classification, Number, and Length of Focal Adhesions

Analysis of microscopic images was performed manually by use of the ImageJ software tools (v.1.51j8; National Institutes of Health). To examine the effect of *HS2ST1* variants on location of paxillin-containing focal adhesions (FAs), we classified FAs as "inner" and "outer" FAs based on the classification scheme reported in Legerstee et al.[26] FAs were classified as outer when they were in contact with or located close to the cell membrane. FAs were classified as inner when they were located further inward, with another FA located in between them and the cell membrane. To compare the location of FAs between different fibroblast cell lines, the ratio of inner to outer FAs was determined. The total number of FAs per cell was calculated as the sum of the number of inner and outer FAs. The length of paxillin-positive signals in micrometers was determined by use of the ImageJ tool for measuring distances, and the average length of FAs per cell was calculated. Quantification of inner and outer FAs, the total number of FAs, and FA length was performed in at least six fibroblasts per cell line and experiment (control 1 [experiment #1: 6 cells; experiment #2: 9 cells; experiment #3: 7 cells], control 2 [8; 7; 7], individual 1 [6; 10; 8], individual 2 [6; 10; 7], individual 3 [7; 6; 8]) and a minimum of 21 cells in total per cell line from three independent experiments. The number of analyzed FAs from [number of cells] were for control 1 cell line 1,387 [22], control 2 1,627 [24], individual 1 1,108 [24], individual 2 1,128 [23], and individual 3 1,009 [21].

Table 1. Clinical Features of Individuals with Bi-allelic *HS2ST1* Variants

Individual #	1 (Family 1)	2 (Family 2)	3 (Fetus) (Family 3)	4 (Family 3)
General Information				
HS2ST1 variant(s) (GenBank: NM_012262.4/ NP_036394.1)	c.342delA (p.Val115*), c.527T>C (p.Phe176Ser)	c.59_62delinsGAA (p.Phe20*), c.493G>T (p.Asp165Tyr)	c.567A>C (p.Arg189Ser), homozygous	c.567A>C (p.Arg189Ser), homozygous
Exon(s)	2 and 4	1 and 4	4	4
Ethnicity	white	white	white	white
Consanguinity	no	no	no	no
Sex	female	male	female	male
Pregnancy and Birth				
Perinatal complications	none	none	oligohydramnios	none
Gestational age (weeks)	37 + 3 (Cesarean section)	38	pregnancy termination at gestational week 23 + 2	38 + 2 (Cesarean section)
APGAR	10/10	8/9/10	N/A	6/8/10
Birth weight (z-score)	2,345 g (−1.5 z)	3,080 g (−0.5 z)	N/D	3,020 g (−0.8 z)
Birth length (z-score)	46 cm (−1.5 z)	50 cm (−0.5 z)	N/D	47 cm (−1.9 z)
OFC birth (z-score)	34 cm (−0.1 z)	N/D	N/D	34 cm (−0.7 z)
Last Examination				
Age	5 y	14 y	N/A	5 d
Weight (z-score)	10.8 kg (−3.4 z)	66.4 kg at age 13 y (+1.5 z)	N/A	3.0 kg at age 15 d (−0.9 z)
Height/length (z-score)	101 cm (−2.2 z)	160 cm at age 13 y (+0.1 z)	N/A	47 cm at age 15 d (−2.0 z)
OFC (z-score)	46 cm (−3.4 z)	N/D	N/A	34 cm at age 15 d (−1.1 z)
Neurobiological Features				
Developmental delay/ intellectual disability	severe	mild to moderate	N/A	N/A
Muscular hypotonia	no, muscle tone increased	mild	N/A	severe
Motor development	delayed	delayed	N/A	N/A
Speech impairment	yes (no speech)	yes (delayed; impaired articulation; speaks sentences)	N/A	N/A
Seizures	no	no	N/A	no
MRI scan	hypoplasia of corpus callosum	delayed myelination	N/D	agenesis of corpus callosum
Skeletal Features				
Body	disproportionate short stature with short arms	pectus excavatum	N/D	long trunk
Limbs	flexion contractures of elbow, hip, and knee joints	genu valgum	arthrogryposis with flexion contractures of elbows and hips and extension deformities of knees	arthrogryposis with flexion contractures of elbows, knees, and hips; shortening of the upper arms with exceeding skin folds
Hands and feet	short hands and feet with brachydactyly and broad fingertips and toes; bilateral pes adductus	broad thumbs and toes; prominent fingertip pads; right clubfoot; bilateral pes planovalgus (arthrodesis); camptodactyly of toes II-V on the right and of toe V on the left	supination of both feet; brachydactyly; bilateral pes adductus; broad distal phalanges of fingers and toes, especially of thumbs and halluces	supination of both feet; brachydactyly; bilateral pes adductus; broad distal phalanges of fingers and toes, especially of thumbs and halluces

(*Continued on next page*)

Table 1. ***Continued***

Individual #	1 (Family 1)	2 (Family 2)	3 (Fetus) (Family 3)	4 (Family 3)
X-ray findings	spine: thoracic kyphoscoliosis; barrel-shaped vertebral bodies; narrow spinal canal. pelvis: narrow iliac bones; sub-luxation of left hip joint; small femoral epiphyses; coxa valga. hands: bone age markedly delayed; brachydactyly of all phalanges; the middle phalanges II-IV and proximal phalanx of the thumb short and ovoid; middle phalanx V missing. feet at age 15 months: bone maturation delayed; reduced ossification of middle phalanges	spine: kyphosis of the thoracic spine; scoliosis of the lower lumbar spine to the left due to hemivertebra L5. pelvis: subluxation of the right hip joint. feet: flexion contractures of toes II-V	N/D	babygram: small femoral epiphysis; normal spine
Other Findings				
Urogenital abnormalities	none	unilateral renal agenesis with megaureter and hypoactivity of musculus detrusor; cryptorchidism	bilateral renal agenesis; rudimentary bladder	left kidney agenesis
Hearing	sensorineural hearing impairment	normal	N/A	otoacoustic emissions not present
Vision	visual impairment	mild myopia	N/A	posterior embryotoxon; hypoplasia of the iris; anterior polar cataract
Feeding	mainly mushy food	normal	N/A	poor sucking ability
Craniofacial dysmorphism	prominent forehead; bitemporal narrowing; hypertelorism; bilateral epicanthus; upslanted palpebral fissures and narrow palpebral fissure (left eye); broad nasal tip; wide mouth; submucous cleft palate; low-set, dysmorphic ears	coarse face; upslanted palpebral fissures; broad nasal tip; wide mouth; full lips; deep philtrum	coarse face; wide-set eyes; thin upper and lower lip vermilion; low-set and posteriorly rotated ears	coarse face; broad forehead; bitemporal narrowing; high frontal hairline; fair hair; periorbital fullness; short and upslanted palpebral fissures; prominent infraorbital fold; broad nasal root, bridge and nasal tip; long and deep philtrum; wide mouth; macroglossia; thin upper lip vermilion; everted lower lip vermilion, pointed chin with retrognathia; full and sunken cheeks; short neck; low-set, posteriorly rotated ears with squared superior portion of helices and prominent crus of helices; attached earlobes
Teeth	N/D	small teeth	N/A	N/A
Additional findings	dystrophy	constipation; two additional nipples	none	capillary hemangiomas on the left side of the face, on the left butt cheek, and of the popliteal fossa

Abbreviations: d, days; m, months; N/A, not applicable; N/D, no data; OFC, occipital-frontal circumference; y, years; z, z-score.

Results

Identification of Bi-allelic Variants in *HS2ST1* in Three Unrelated Affected Individuals with Developmental Delay, Corpus Callosum Hypoplasia or Aplasia, and Skeletal and Renal Abnormalities

We investigated family 1 with one affected girl (individual 1), first seen at age 3 years and 6 months (Figure 1 and Table 1). She was born to a non-consanguineous couple at 37 + 3 weeks of gestation by Cesarean section with measurements in the lower normal range for length and weight and mean occipito-frontal head circumference (OFC). Her psychomotor development during infancy and early childhood was severely delayed. Brain MRI at age 3 years revealed partial agenesis of the corpus callosum with absent body and splenium and hypoplastic rostrum and genu. Facial dysmorphism at the age of 3.5 years comprised scaphocephaly, prominent forehead with bitemporal

narrowing, hypertelorism, upslanted and asymmetric palpebral fissures with a left narrow one, bilateral epicanthus, broad nasal root and tip, wide mouth, and low-set, dysmorphic ears (Figures 2A and 2B). On last examination at age 5 years, her length was 101 cm (−2.2 z), weight was 10.8 kg (−3.4 z, according to length), and OFC was 46 cm (−3.4 z). Apart from dystrophy and disproportionate short stature with short appearing limbs, she had kyphoscoliosis, flexion contractures of elbow, hip, and knee joints, brachydactyly of hands and feet, and broad fingertips and toes (Figures 2C–2E). Muscle tone was increased, and her motor and cognitive development severely delayed. She could not speak. Her vision appeared to be impaired, though ophthalmologic examination—including fundoscopy and visually evoked potentials—revealed normal results. Ear-nose-throat studies disclosed submucous cleft palate and mucotympanum causing reduced conduction; in addition, a sensorineural component of hearing impairment was diagnosed. Radiologic studies of the spine, pelvis, hand, and foot at different ages revealed thoracic kyphoscoliosis with anteriorly rounded (barrel-shaped) vertebral bodies (Figures 3A and 3B), subluxation of the left hip joint, bilateral small femoral epiphyses, and coxa valga (Figure 3C). Hand X-ray demonstrated camptodactyly and brachydactyly, markedly delayed bone maturation, and short phalanges with particularly short and plump (ovoid) middle phalanges (Figure 3D). Bone maturation of the foot was also delayed, and the rudimentary middle phalanges were almost unossified (Figure 3E). We performed WES in individual 1 and her healthy parents and identified the compound heterozygous variants c.342delA, predicting the introduction of a premature stop codon (p.Val115*), and c.527T>C, predicting the amino acid substitution p.Phe176Ser, in *HS2ST1* (Figures 1 and S1A and Table S2). Both variants are absent in public databases including the gnomAD browser (Table S2). The genetic variants were validated in individual's 1 DNA using Sanger sequencing. Her father was a heterozygous carrier of the 1-bp deletion and her mother of the c.527T>C change (Figures 1 and S1A).

Through GeneMatcher,[27] we identified two unrelated families with three affected individuals harboring bi-allelic variants in *HS2ST1* (Figure 1). Individual 2 (family 2), a 14-year-old boy, carried the compound heterozygous variants c.59_62delinsGAA (p.Phe20*) and c.493G>T (p.Asp165Tyr) (Figure 1 and Table S2). The c.59_62delinsGAA variant is absent in public databases, and the c.493G>T change is listed twice in the heterozygous state in gnomAD (MAF: 0.0008695%; Table S2). The c.59_62delinsGAA variant was inherited from the mother, and the p.Asp165Tyr variant was paternally inherited. The healthy older brother of individual 2 carried the *HS2ST1* missense variant in the heterozygous state (Figure 1). Individual 2 was born after an uneventful pregnancy at gestational age of 38 weeks with a birth weight of 3,080 g (−0.5 z) and length of 50 cm (−0.5 z) (Table 1). Shortly after birth, clubfoot on the right and bilateral cryptorchidism was noted. Within the neonatal period he developed an urosepsis, and unilateral kidney agenesis was identified. He was first seen at the Clinical Genetics outpatient clinic at the age of 3 months. He is the second child of non-consanguineous parents. Family history did not reveal any relevant conditions. Upon physical examination his height, weight, and OFC were all normal. Radiologic studies at the age of 6 years revealed kyphosis of the thoracic spine and scoliosis of the lower lumbar spine due to hemivertebra L5 (Figures 3F and 3G). X-rays of feet demonstrated flexion contractures of the 2nd to 5th toes (Figures 3H and 3I). Facial dysmorphism at the age of 10 years comprised coarse face, upslanted palpebral fissures, broad nasal tip, wide mouth with full lips, deep philtrum, and high palate (Figures 2F and 2G). He had broad thumbs and toes and bilateral pes planovalgus (Figures 2H and 2I), prominent fingertip pads, and a small umbilical hernia. Upon follow up, his development was delayed. At the age of 14 years, he walked with a walker, spoke with limited articulation, had a considerable vocabulary, and was able to read. Metabolic screen of urine, plasma, and cerebrospinal fluid did not show any abnormalities. Furthermore, he had small teeth and detrusor underactivity (Table 1).

In the third family, the homozygous *HS2ST1* missense variant c.567A>C (p.Arg189Ser) (absent in gnomAD) was identified in a fetus (individual 3) after induced abortion at 23 + 2 weeks of gestation (Figure 1 and Table S2). Both healthy parents were heterozygous carriers of the *HS2ST1* missense change (Figure 1). The female fetus was the first child of non-consanguineous parents with unremarkable family history (Table 1). Until gestational week 16, the pregnancy was uneventful. Severe oligohydramnion was detected at week 21, and bilateral kidney agenesis was suspected. Autopsy showed a fetus who was too small for gestational age with fixed flexion contractures of the elbows and hips, extension deformities of knees, and supination of both feet with bilateral pes adductus with broad and medially deviated halluces. The hands appeared short, and both thumbs were broad and short. Eyes appeared wide-set, the upper and lower lip vermilion was thin, and ears were low-set and posteriorly rotated (Figure 2J). Further autoptic findings were a single umbilical artery, bilateral kidney agenesis, a rudimentary bladder, and unlobulated lungs (Table 1). Individual 4 was the younger brother of individual 3 and also carried the *HS2ST1* p.Arg189Ser variant in the homozygous state (Figure 1, Tables 1 and S2). He was born at 38 + 2 weeks of gestation by Cesarean section. During pregnancy corpus callosum agenesis and unilateral kidney agenesis were suspected by ultrasound in week 21 of gestation and confirmed by fetal MRI. At birth, his weight was 3,020 g (−0.8 z), length was 47 cm (−1.9 z), and OFC was 34 cm (−0.7 z). His APGAR scores were 6, 8, and 10 at 1, 5, and 10 min of life. He was admitted to the neonatal intensive care unit for 15 days and received cardiorespiratory and feeding support. He had a coarse facial appearance with broad

forehead, bitemporal narrowing with deep-set eyes, short, upslanted palpebral fissures, periorbital fullness, prominent infraorbital fold, broad nasal root, bridge, and tip, full and sunken cheeks, long and deep philtrum, wide mouth, macroglossia, thin upper vermilion with exaggerated cupid-bow, everted thick lower vermilion, pointed chin, retrognathia, low-set, posteriorly rotated ears, squared superior portion of helices, prominent crus of helices, attached earlobes, and short neck (Figure 2K). He had capillary hemangiomas on the left side of the face, extending from the temporal region to the supraorbital region, left side of the nose and cheek, on the left butt cheek, and the left popliteal fossa. Limbs showed arthrogryposis with flexion contractures of elbows, knees, and hips. Supination of both feet, brachydactyly with broad fingertips and toes, broad distal phalanges of finger and toes, especially of thumbs and halluces, bilateral pes adductus (Figures 2L and 2M), and apparently shortening of the arms with exceeding skin folds were observed. Ophthalmologic examination revealed a posterior embryotoxon, hypoplasia of the iris, and anterior polar cataract. Abdominal ultrasound confirmed left kidney agenesis. Otoacoustic emissions were not present, and weight gain was difficult because of poor sucking (Table 1).

HS2ST1 is intolerant to functional genetic variation, as only 69% of the expected missense (observed/expected score: 0.69) and 20% of the expected loss-of-function variants (observed/expected score: 0.2) were found in gnomAD,[28] further indicating a pathogenic role of the *HS2ST1* variants in the affected individuals. The *HS2ST1* missense variants p.Asp165Tyr, p.Phe176Ser, and p.Arg189Ser were predicted to have a damaging impact on protein function by three *in silico* tools and affect an intolerant amino acid residue each (Table S2). Together, based on rarity or absence of the identified *HS2ST1* variants in population databases, two likely truncating variants, three missense variants with a possible damaging effect on enzymatic activity, as well as overlapping clinical features in the four affected individuals, we believe the bi-allelic *HS2ST1* variants to underlie the phenotype in all of them. This is further underscored by renal, skeletal, and eye abnormalities in *Hs2st1* knockout mice,[17] showing similarities with the clinical manifestations of the fetus and the three live individuals described here.

Reduced *HS2ST1* mRNA Levels and Decreased or Absent HS2ST1 Protein in Fibroblast Cells of Two Affected Individuals

To characterize the effect of compound heterozygous and homozygous *HS2ST1* variants on transcript and protein level, we used fibroblasts derived from individuals 1, 2, and 3. We first PCR-amplified fibroblast-derived cDNA from the three individuals and Sanger-sequenced the PCR products to identify possible aberrant *HS2ST1* mRNAs. In individual 1, we found predominant abundance of *HS2ST1* transcripts with the c.527T>C variant suggesting nonsense-mediated mRNA decay (NMD) of mRNAs harboring the c.342delA deletion (Figure S1A). In contrast, in fibroblast-derived cDNA of individual 2, *HS2ST1* transcripts with the delins variant and the c.493G>T change were detectable in equal amount suggesting no efficient clearance of *HS2ST1* mRNAs with the c.59_62delins variant by NMD (Figure S1B). As expected, *HS2ST1* cDNA analysis in individual 3 revealed the presence of mRNAs with the c.567A>C change (Figure S1C).

We next determined the relative levels of *HS2ST1* mRNA in cells of affected individuals by RT-qPCR. *HS2ST1* mRNA amount was reduced to ~53% and ~64% in fibroblasts of individuals 1 and 2, respectively, compared to control 1 cells (~50% and ~61% compared to control 2 cells; Figures 4A and S2). This is in line with data from qualitative *HS2ST1* transcript analysis in cells of individual 1 and underscores NMD of mRNAs harboring the premature stop codon p.Val115* (Figure S1A). In contrast, reduced *HS2ST1* mRNA amount in individual 2 cells is possibly due to a decay of both mutant mRNAs as the delins and the c.493G>T variants were present in the RT-PCR amplicon sequences (Figure S1B). The level of *HS2ST1* mRNA in cells of affected individual 3 was comparable to that of control cells (~93% and ~88% compared to control 1 and 2, respectively), suggesting stability of *HS2ST1* transcripts harboring the missense variant p.Arg189Ser (Figure 4A).

We used whole-cell lysates from primary fibroblast cultures for HS2ST1 protein analysis via immunoblotting. HS2ST1 was almost completely absent in fibroblasts of individual 2 (Figures 4B, 4C, and S3). The remaining protein was ~7% in cells of individual 2 compared to cells of controls 1 and 2 (Figure 4C). In cells of individual 1, the HS2ST1 protein level correlated well with the determined transcript amount: 49%–52% of HS2ST1 protein was found in fibroblasts of individual 1 compared to control 1 and 2 cells (Figure 4C). All *HS2ST1* mutant transcripts in individual 3 cells seemed to give rise to protein as the same amount of HS2ST1-Arg189Ser mutant protein was detected in individual 3 cells compared to wild-type HS2ST1 in control 1 cells (Figures 4B and 4C). Together, the data suggest that both the C-terminally truncated HS2ST1-Phe20* and the HS2ST1-Asp165Tyr mutant proteins in individual 2 cells show intrinsic instability and/or are subject to enhanced degradation, while HS2ST1 protein with the amino acid change p.Phe176Ser or p.Arg189Ser seems to be stable in fibroblast cells. Together with data from structural and mutation analysis of HS2ST1[12,13] (see above), the substitutions p.Phe176Ser and p.Arg189Ser likely have a negative impact on HS2ST1's enzymatic activity rather than on protein stability.

Heparan Sulfate from Fibroblasts of Individual 1 Lacks 2-*O*-Sulfation and Shows an Increase in *N*- and 6-*O*-Sulfation

HS is a highly sulfated linear polysaccharide that undergoes a series of modifications during its biosynthesis. These modifications transform a uniform *N*-acetyl

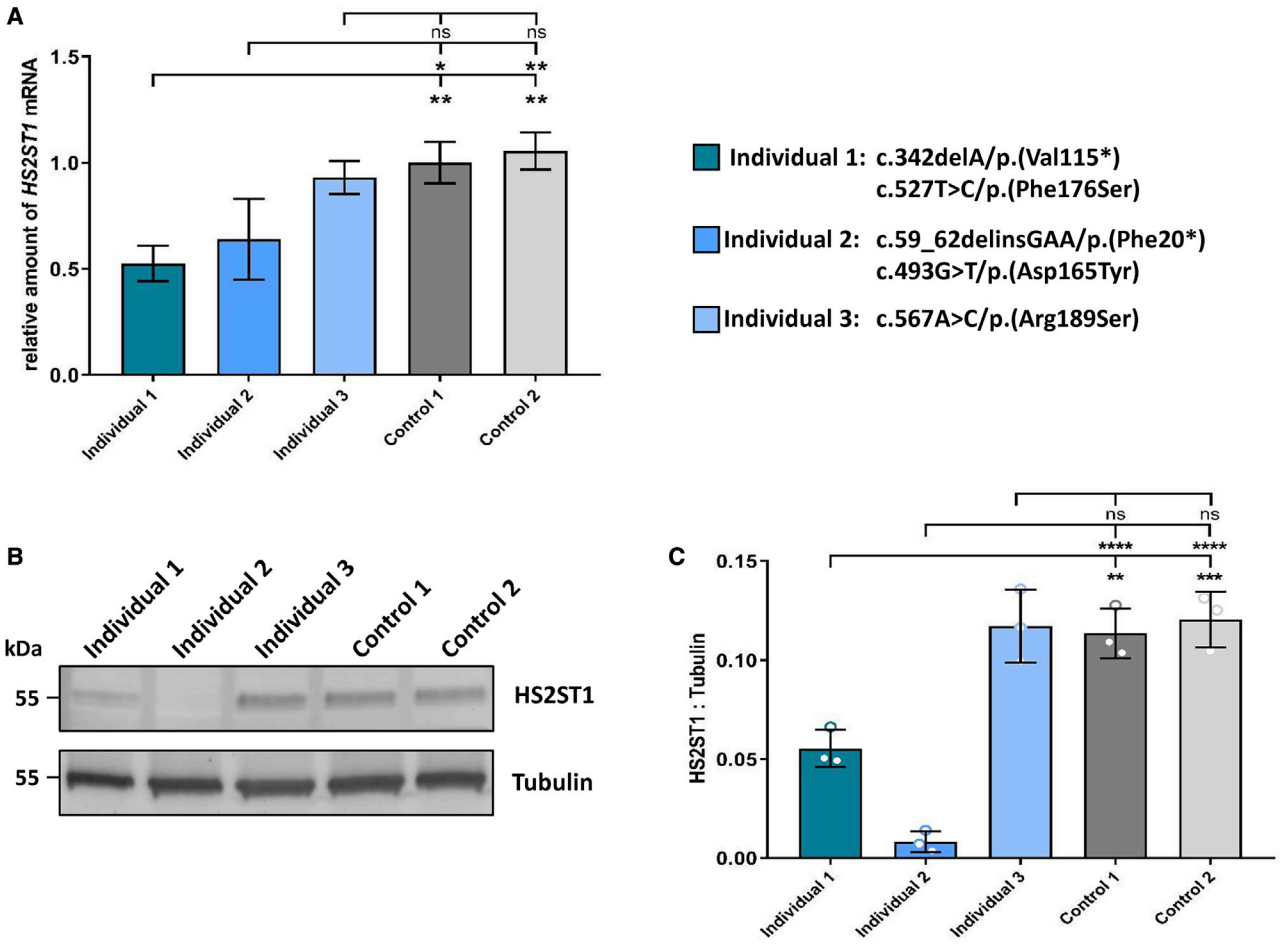

Figure 4. Determination of HS2ST1 mRNA and Protein Amount in Fibroblasts from Affected Individuals

(A) Quantification of *HS2ST1* transcripts by RT-qPCR. RNA was obtained from fibroblasts of individuals 1, 2, and 3 and two healthy individuals (control). *GAPDH* mRNA was used as an internal control, and the amount of *HS2ST1* mRNA relative to *GAPDH* mRNA is presented. *HS2ST1* variants found in the three individuals are shown on the right. The mean of three independent experiments ± SD is given. Mean of technical duplicates from each experiment is shown in Figure S2.

(B) Immunoblot of lysates obtained from fibroblasts of three affected individuals and two control subjects. The amount of HS2ST1 protein was monitored with an anti-HS2ST1 antibody, and an anti-tubulin antibody was used for equal loading. Uncropped blots are shown in Figure S3.

(C) Band intensities of fluorescence signals were quantified using the ChemiDoc imaging system. The mean of three independent experiments ± SD is given. One-way ANOVA with Bonferroni correction was used for statistical analysis: *$p \leq 0.05$; **$p \leq 0.01$; ***$p \leq 0.001$; ****$p \leq 0.0001$; ns, not significant.

glucosamine (GlcNAc)-glucuronic acid (GlcA) polymer to a complex mature HS chain with alternating high-sulfated and low-sulfated domains. *N*-sulfation of specific glucosamine residues converts clusters of GlcNAc residues to *N*-sulfated glucosamine (GlcNS)-rich regions. This is followed by epimerization of selected glucuronic acid (GlcA) residues to form iduronic acid (IdoA) and further *O*-sulfation including 2-*O*-sulfation (2S), primarily of IdoA residues (IdoA(2S)), 6-*O*-sulfation (6S), and rarely 3-*O*-sulfation (3S) of GlcNS/GlcNAc.[1] Structural analysis of embryonic fibroblast HS of the *Hs2st1* knockout mouse demonstrated increased *N*- and 6-*O*-sulfation in the absence of any 2S. A particular increase in uronic acid (UA)-GlcNS and UA-GlcNS(6S) residues of the HS chains has been identified.[19] To determine whether a similar shift in global sulfation patterning occurred in fibroblasts of individuals with bi-allelic *HS2ST1* variants, we carried out disaccharide compositional analysis on HS isolated from fibroblasts expanded in culture. We were able to isolate sufficient HS from cell lysates and conditioned media of individual 1 and two controls to carry out compositional analysis, but not from fibroblasts of individuals 2 and 3. Cell lysate and conditioned media HS was analyzed separately and compared against equivalent material isolated from control cells. In both cell lysate and conditioned media material from individual 1, 2S was significantly reduced compared to controls (Figures 5A–5D). Specifically, total 2S was 0.6% in individual 1 cell lysate compared to 15% in both control cell lysates (Figure 5C). Similar differences were observed in conditioned media (individual 1 conditioned media 2%; control 1 11%; control 2 8%; Figure 5D). The 2S trace level seen in conditioned media

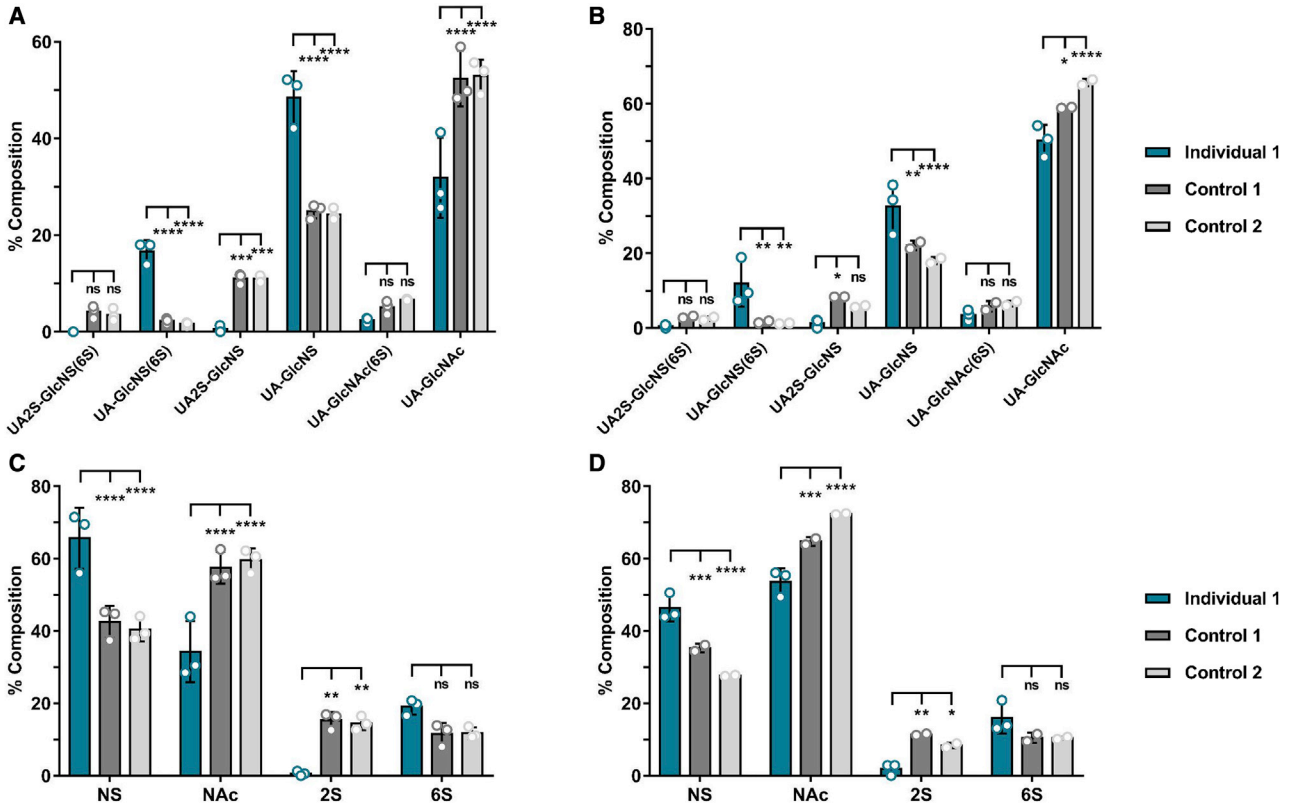

Figure 5. Comparative Disaccharide Composition of Heparan Sulfate from Lysates and Conditioned Media of Fibroblasts of Individual 1 and Two Control Subjects

From the disaccharide analysis (cell lysate in A and conditioned media in B), the total levels of *N*-sulfation (NS), *N*-acetylation (NAc), 2-*O*-sulfation (2S), and 6-*O*-sulfation (6S) of isolated heparan sulfate chains could be calculated (cell lysate in C and conditioned media in D) and are represented in the above charts. Results are an average of three (cell lysate and media from individual 1, cell lysate from controls 1 and 2) or two (media from controls 1 and 2) independent samples (mean ± SD). Two-way ANOVA with Tukey correction was used for statistical analysis: *p ≤ 0.05; **p ≤ 0.01; ***p ≤ 0.001; ****p ≤ 0.0001; GlcNAc, *N*-acetyl glucosamine; GlcNS, *N*-sulfated glucosamine; ns, not significant; UA, uronic acid.

of individual 1 cells was likely due to HS present in the serum (serum-containing media not exposed to cells was found to have 6% 2S; Figure S4). Remarkably, we observed a similar increase in *N*-sulfation (NS) and 6-*O*-sulfation (6S) as seen in the *Hs2st1* knockout mouse with cell lysate of individual 1 HS having 19% 6S and 66% NS compared to 12% 6S in both controls and 45% and 40% NS in control 1 and 2, respectively (Figures 5A and 5C). A similar pattern of altered sulfation was seen in HS isolated from the conditioned media (Figures 5B and 5D), with increases in UA-GlcNS(6S) and UA-GlcNS seen in both cell lysate and conditioned media of individual 1 (Figures 5A and 5B). The data indicate a strongly diminished or nearly absent 2-*O*-sulfotranserase activity in cells derived from individual 1 with the bi-allelic *HS2ST1* variants p.Val115* and p.Phe176Ser.

Reduced FGF-2-Induced Activation of the MAP Kinases ERK1/2 and Restoration of the FGF-2 Stimulatory Activity by Heparin Addition to Fibroblasts of Affected Individuals

HS modulates FGF signaling by concomitantly interacting with both the growth factor and the receptor to form a ternary complex.[29,30] For optimal interaction between the three molecules, 2-*O*-sulfation of HS is an essential requirement.[6,7] In line with this, the aberrant HS from *Hs2st1*$^{-/-}$ mice has a reduced affinity for FGF-1 and FGF-2; however, embryonic fibroblasts from these mice were still able to signal in response to these factors, possibly as a result of the concomitant increase in *N*- and 6-*O*-sulfation.[19] MAP kinase signaling, e. g. dual phosphorylation of ERK1/2, is one well-studied pathway to assess the dependence of HS for FGF binding and activation of cell-surface FGF receptors.[19,31,32] We next determined the phosphorylation status of ERK1/2 in serum-starved fibroblasts that were treated with FGF-2 for 10 or 20 min. We identified an increase over baseline in ERK1/2 phosphorylation after 10 and 20 min of FGF-2 stimulation for all cell lines (Figures 6A and S5). However, the response to FGF-2 was significantly less in cells of affected individuals (Figure 6A, compare upper with lower panel). ERK1/2 phosphorylation after 10 min of FGF-2 treatment was 1.5- to 1.7-fold lower in cells from individuals 1, 2, and 3 than in control 1 fibroblasts (and 1.4- to 1.5-fold lower than in control 2 fibroblasts; Figure 6B). Similarly, after 20 min of FGF-2 treatment, the phosphorylation level of

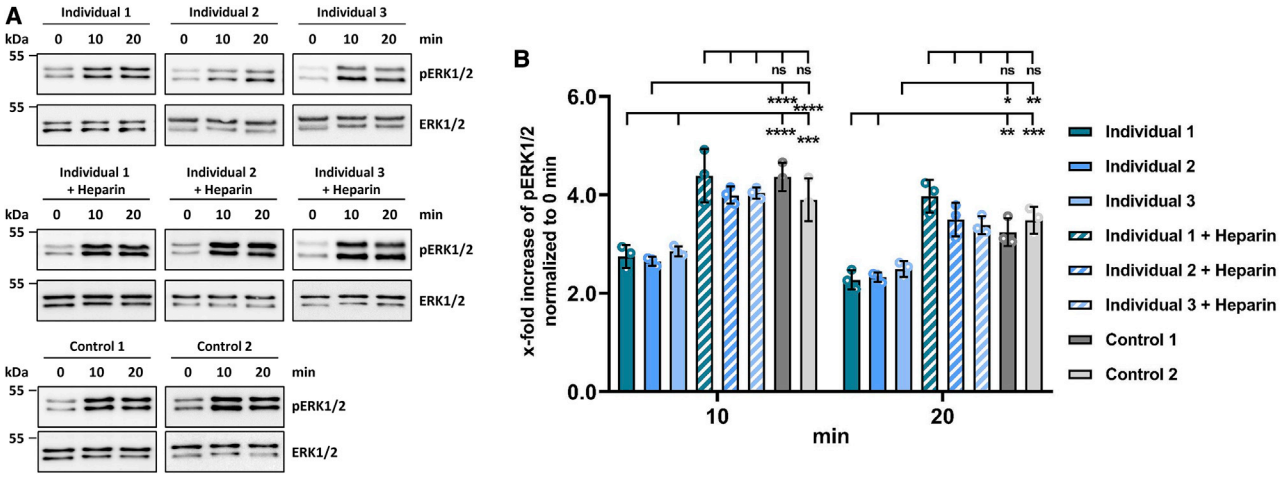

Figure 6. Effect of FGF-2 and Heparin Treatment on ERK1/2 Activation in Fibroblasts from Affected Individuals
(A) Immunoblot of lysates obtained from fibroblasts of individuals 1, 2, and 3 and two controls. After serum starvation overnight, cells were stimulated with 10 ng/mL FGF-2 (upper and lower panels) or 10 ng/mL FGF-2 and 30 ng/mL heparin (middle panel) for 0–20 min as indicated. Endogenous phosphorylated ERK1/2 (pERK1/2) and total ERK1/2 were detected in whole cell lysates by immunoblotting. Representative blots are shown; uncropped blots are shown in Figure S5.
(B) Band intensities of fluorescence signals were quantified using the ChemiDoc imaging system. pERK1/2 was normalized to total ERK1/2, and the ratio at 0 min was set to 1. The mean of three independent experiments ± SD is given. Two-way ANOVA with Tukey correction was used for statistical analysis: *$p \leq 0.05$; **$p \leq 0.01$; ***$p \leq 0.001$; ****$p \leq 0.0001$; ns, not significant.

ERK1/2 was significantly reduced by 1.3- to 1.5-fold in the three cell lines derived from affected individuals compared to control 1 and 2 cells (Figure 6B). Together, these data demonstrate a significantly reduced FGF-2-dependent MAPK signaling response in cell lines of the three affected individuals pointing to a possible requirement of 2-*O*-sulfated HS for normal FGF-2-induced signaling in these cells.

To determine whether the diminished stimulatory effect of FGF-2 in fibroblasts of affected individuals can be restored by exogeneous (commercially available) heparin, a GAG with similar structure to HS,[33,34] we simultaneously added FGF-2 and heparin to the cell culture medium and determined ERK1/2 phosphorylation in cells of affected individuals. After 10 and 20 min of treatment, the growth stimulatory effect of FGF-2 was completely restored as the level of ERK1/2 phosphorylation was almost the same in all three cell lines derived from affected individuals compared to control cells stimulated only with FGF-2 (Figure 6A, compare middle with lower panel, and Figure 6B). We next added heparin alone to fibroblasts of affected individuals and measured ERK1/2 phosphorylation. Similar to the treatment of cells of affected individuals with FGF-2 alone, addition of heparin resulted in an increase over baseline of ERK1/2 phosphorylation in these cells; however, the ERK1/2 phosphorylation level was only 1.2- to 1.5-fold and 1.3- to 1.4-fold higher after 10 min and 20 min, respectively, of heparin treatment in cells of affected individuals (Figure S6) (compared to 2.6- to 2.8-fold and 2.3- to 2.5-fold higher ERK1/2 phosphorylation after 10 min and 20 min, respectively, of FGF-2 stimulation; Figures 6A and 6B). These results demonstrate that optimal ERK1/2 activation in fibroblasts of individuals with bi-allelic *HS2ST1* variants requires both FGF-2 and the GAG heparin.

Focal Adhesions Concentrate at the Cell Periphery in Fibroblasts of Individuals with Bi-allelic *HS2ST1* Variants

As well as interacting with HPSGs as co-receptors, FGF-2 can additionally interact with other GAGs, such as chondroitin sulfate and dermatan sulfate, to activate multiple signaling pathways.[35,36] For example, FGF-2 has been found to trigger actin cytoskeletal dynamics, such as cell migration and focal adhesion formation.[37–39] Focal adhesion formation requires the local recruitment of focal adhesion proteins, such as focal adhesion kinase, vinculin, and paxillin.[40,41] Interestingly, soluble HS fragments enhance the formation and activation of focal adhesions,[42,43] and FGF-2 together with 2-*O*-sulfated chondroitin sulfate and/or dermatan sulfate affect the formation of focal adhesion complexes, paxillin activation, and cell migration.[44] We next examined the effect of FGF-2 stimulation on position, number, and length of focal adhesions (FAs) in fibroblasts from individuals with bi-allelic *HS2ST1* variants and two controls. Cells were stimulated with FGF-2 and stained for the FA marker paxillin. In control cells, paxillin appeared as dot-like or elongated structures distributed throughout the basal surface and at the cell periphery (Figures 7A and S7), while FAs in cells derived from affected individuals concentrated at the cell periphery, with fewer paxillin-positive structures at the basal surface (Figures 7A and S7). We did not observe any difference in the total amount of paxillin in cell lysates of affected individual- and control-derived cells (Figure S8). We next classified FAs as outer and inner FAs (Figure 7B and Subjects and

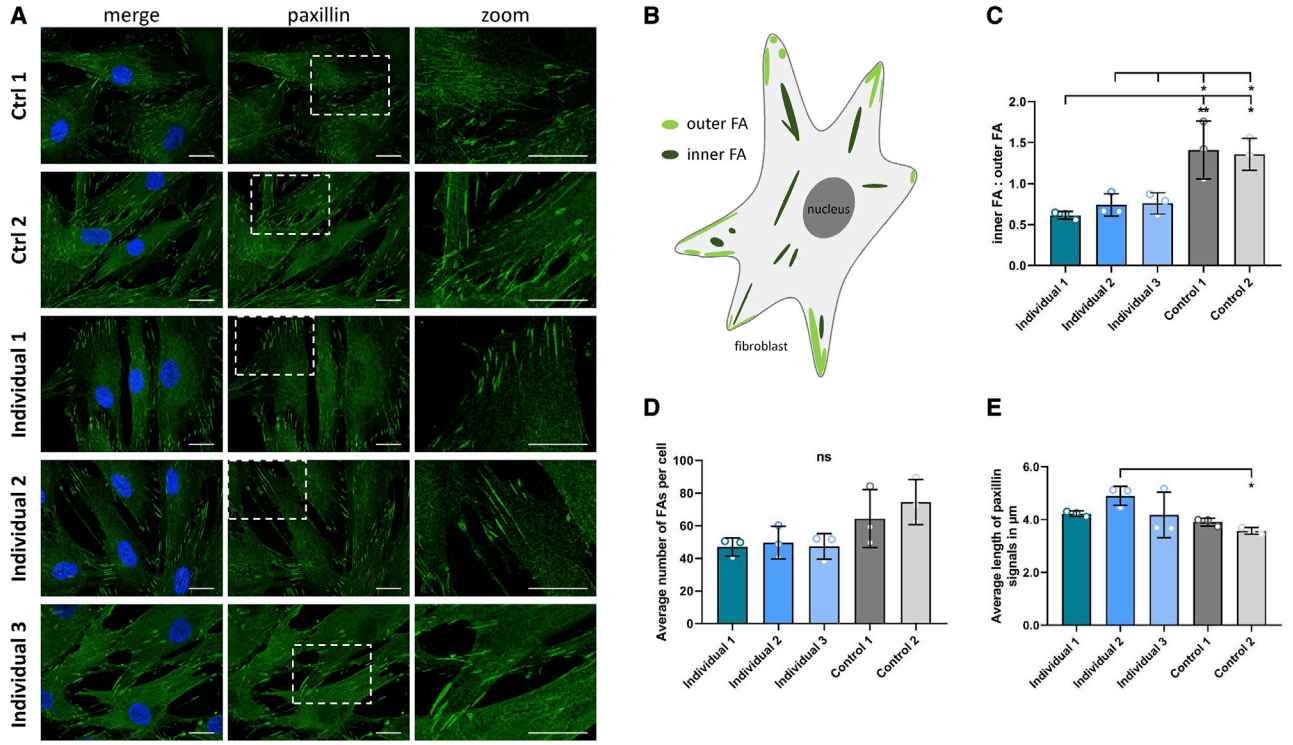

Figure 7. Change in Location, but Not Length and Number of Paxillin-Positive Focal Adhesions in Fibroblasts from Affected Individuals

(A) Fibroblasts were seeded on coverslips and incubated with 10 ng/mL FGF-2 for 1 h. Paxillin was stained by mouse anti-paxillin antibody followed by anti-mouse Alexa Fluor488-conjugated antibody (green). Nuclear DNA was labeled by DAPI (blue). Cells were imaged by widefield fluorescence microscopy. Representative images are shown. A magnified view of the boxed region is shown on the right. Scale bar, 20 μm. Ctrl 1 and 2, control fibroblasts.

(B) Schematic illustration of the categorisation of focal adhesions (FAs) based on distance from the cell membrane (modified according to Legerstee et al.[26]). FAs were classified as outer (light green) and inner (dark green) FAs (see Subjects and Methods section for details).

(C) Quantification of inner and outer FAs in FGF-2-treated fibroblasts. The ratio of inner to outer FAs per cell in each experiment was determined, and the mean ratio of three independent experiments ± SD is given. One-way ANOVA with Bonferroni correction was used for statistical analysis: *$p \leq 0.05$; **$p \leq 0.01$.

(D and E) Quantification of the number and length of FAs in FGF-2-treated fibroblasts. The total number of paxillin-positive FAs (D) and the FA length (E) of at least 6 cells per cell line and experiment and a minimum of 21 cells in total per cell line from three independent experiments were determined (see Subjects and Methods for details). The mean number of FAs per cell ± SD (D) and the average length of FAs ± SD (E) are illustrated. One-way ANOVA with Bonferroni correction was used for statistical analysis: *$p \leq 0.05$; ns, not significant.

Methods) and determined the ratio of inner to outer FAs in each cell line. The inner to outer FA ratio was reduced by 1.8- to 2.3-fold in the three cell lines derived from affected individuals compared to control 1 and 2 cells (Figure 7C). The average number of FAs per cell and the average length of FAs were similar in fibroblasts from individuals 1 to 3 and controls (Figures 7D and 7E). These data indicate a change in the location of paxillin-positive FAs in the three cell lines of affected individuals compared to control cells.

Discussion

Here we demonstrate bi-allelic pathogenic variants in *HS2ST1* to be the underlying genetic cause for a syndromic phenotype characterized by developmental delay and/or intellectual disability, hypoplastic or absent corpus callosum, facial dysmorphism with upslanted palpebral fissures, broad nasal tip, and wide mouth, skeletal abnormalities, and uni- or bilateral renal agenesis. Two affected individuals carried compound heterozygous *HS2ST1* variants with a loss-of-function variant in combination with a missense change. In the third family, a severely affected fetus and a male newborn were homozygous for the missense variant p.Arg189Ser. The three substituted amino acid residues Asp165, Phe176, and Arg189 are located in or near the binding cleft for the saccharide substrate of the sulfotransferase (Figure 2B in Bethea et al.[12] and Figure 3 in Liu et al.;[45] Figure S9). Structural and mutation analysis of HS2ST1 revealed several amino acid residues to be important for binding to PAPS and the polysaccharide substrate as well as for catalytic activity.[12,13] Arginine 164 is located next to aspartate 165 which is substituted to tyrosine in individual 2. The HS2ST1 p.Arg164Ala mutant showed a significantly decreased enzyme activity and abolished binding to 3′-phosphoadenosine 5′-phosphate (PAP), the product of sulfotransferase-catalyzed reactions.[13] The p.Asp165Tyr change may have a similar effect as the p.Arg164Ala

substitution. Arginine 178 is implicated in substrate binding, and the HS2ST1 mutant p.Arg178Ala showed a significant decrease in both enzyme activity and PAP binding.[13] Similarly, tyrosine 173 is also in contact with the saccharide substrate.[45] In individual 1, exchange of phenylalanine 176, located between Tyr173 and Arg178 in the alpha helix 5 region, by serine may weaken the binding affinity of HS2ST1 to the IdoA and/or GlcA residue and reduce sulfotransferase activity. In one study, the p.Arg189Ala substitution resulted in significant loss of HS2ST1 enzyme activity.[13] In two other studies, arginine 189 was found to be important for recognition of IdoA units and substrate specificity.[12,45] Together, structural and mutational data from HS2ST1 revealed that the three residues Asp165, Phe176, and Arg189 are located at structurally and functionally relevant positions, and their substitution may weaken the binding to HS, redirect the substrate specificity, and/or reduce the sulfotransferase activity.[12,13,45]

We demonstrate a low and significantly reduced FGF-2-dependent MAPK signaling response in the three cell lines of affected individuals that can be restored by exogeneous heparin.[29,30] These data show the importance of 2-*O*-sulfated heparin (or HS) for FGF-2-induced MAPK signaling in human skin fibroblasts. In a recent study, the degree of 2-*O*-sulfated cell surface chondroitin and dermatan sulfate has been shown to modulate FGF-2-induced ERK1/2 activation, paxillin activation, and cell migration.[44] We could demonstrate that in FGF-2-stimulated fibroblasts of individuals with bi-allelic pathogenic *HS2ST1* variants, the position of FAs was altered, with a higher density of paxillin-positive structures at the cell periphery compared to control cells. The role of cell membrane-bound GAGs in cytoskeletal organization has previously been demonstrated.[46] For example, an excess of extracellular HS fragments enhances focal adhesion formation and activation,[42] and 2-*O*-sulfation of chondroitin and/or dermatan sulfate is important for mediating cell migration and adhesion.[47–49] Together, the data demonstrate that 2-*O*-sulfated GAGs play an important role in FGF-2-induced cytoskeletal rearrangements; however, more studies are needed to characterize the multiple potential pathways implicated in HSPG-dependent actin cytoskeletal dynamics.

Disaccharide analysis of HS from fibroblasts of one individual with bi-allelic *HS2ST1* variants revealed lack of 2-*O*-sulfation and increase in *N*- and 6-*O*-sulfation. Thus, retention of a normal charge distribution of the aberrant HS seems to maintain normal FGF-1 and FGF-2 signaling response in *Hs2st1*-deficient mouse embryonic fibroblasts[19] but is unable to achieve the same level of compensation in human fibroblasts deficient of 2-*O*-sulfotransferase 1 activity. In Chinese hamster ovary cells, the structure and organization of highly sulfated domains rather than the fine structure of HS were found to be critical for FGF-2 signaling.[32] However, the phenotype of *Hs2st1*-deficient mouse embryos and individuals with bi-allelic *HS2ST1* pathogenic variants indicates that the aberrantly synthesized HS is not able to compensate for the lack of 2-*O*-sulfated HS in a number of cells and tissues during development (this work and Merry and Wilson[18]).

The core phenotype associated with bi-allelic *HS2ST1* variants in the four affected individuals comprises developmental delay and/or intellectual disability, corpus callosum hypoplasia or agenesis, facial dysmorphism, flexion contractures, and broad toes and/or finger tips, especially of thumbs and halluces. Bilateral renal agenesis was present in individual 3 and unilateral renal agenesis in individuals 2 and 4 (Table 1). Several of the clinical features observed in the affected individuals were also present in *Hs2st1* knockout mice, although mutant animals were more severely affected. *Hs2st1*-deficient mice show neonatal lethality. All mutant mice have bilateral renal agenesis,[17] suggesting that 2-*O*-sulfation critically modulates the activity of one or more growth factors involved in kidney development.[19] Indeed, HS modifications by Hs2st1 have been shown to influence the binding of growth factors involved in metanephric mesenchyme induction and differentiation in the developing kidney, while 6-*O*-sulfated HS is important for growth and branching of the ureteric bud.[50,51] These data suggest that differentially sulfated HS controls morphogen activity and function and acts as a switch during the development of specific organs.[50] *Hs2st1* knockout mice show abnormalities of the skeleton, such as an increase in bone mineralization, shorter and thicker long bones, and ~55% have post-axial polydactyly of one forelimb.[17] In the affected individuals reported here, various skeletal anomalies have been observed, including flexion contractures, short hands and feet with brachydactyly, broad fingertips and toes, clubfoot, supination of feet, kyphoscoliosis, and delayed bone maturation. None of the four affected individuals had polydactyly. In chick embryos, downregulation of *HS2ST1* expression resulted in limb buds that were truncated and reduced in size, while mildly affected forelimbs showed a defective digit and size reduction, demonstrating the requirement of HS 2-*O*-sulfation for limb development.[52] About 40% of the *Hs2st1*-deficient mice had secondary cleft palate.[17] A submucous cleft palate was also reported in individual 1 (Table 1). Bilateral iris coloboma was seen in all homozygous *Hs2st1* knockout mice and cataract in six of eight mutants.[17] Individuals 1 to 3 did not have any ophthalmological anomalies; however, posterior embryotoxon, iris hypoplasia, and an anterior polar cataract were observed in individual 4 (Table 1). Two of the four affected individuals had agenesis or hypoplasia of the corpus callosum. Hs2st1 is expressed in the developing telencephalon, and *Hs2st1*$^{-/-}$ mouse embryos have severe corpus callosum phenotypes, but with incomplete penetrance: axons failed to cross the telencephalic midline and form knotted bundles.[53] More detailed analysis revealed a repressive function of Hs2st1-modified HS on Fgf/Erk signaling in the embryonic telencephalic midline, likely by specific suppression of Fgf17 protein levels in the corticoseptal boundary.[54,55] Thus, the similar

corpus callosum abnormalities in mice and humans deficient of *HS2ST1* identify an important role for the 2-*O*-sulfotransferase 1 in the developing mammalian telencephalon by tightly controlling MAP kinase signaling. In summary, data from animal and human studies indicate the requirement of 2-*O*-sulfated HS for morphogenesis of a number of organs during vertebrate development. Further support for these findings comes from studies of a knockout mouse for the D-glucuronyl C5-epimerase (Glce) encoding gene.[56] The protein is one of the specialized enzymes involved in HS synthesis and catalyzes the C5-epimerization of GlcA to IdoA, with IdoA being preferentially 2-*O*-sulfated by HS2ST1.[1] *Glce*-deficient mice show considerable phenotypic overlap with *Hst2st*$^{-/-}$ mice as they die after birth, lack kidneys, and show bilateral colobomas and skeletal abnormalities.[56] Interestingly, *Glce*$^{-/-}$ embryos lack some phalanges of the fore and hind paws and often have cleft palate which is reminiscent of shortened or missing phalanges of the hand (Figure 3D) and submucous cleft palate in individual 1 reported here. Collectively, the data show that HS with 2-*O*-sulfated IdoA residues is important for murine kidney, iris, and skeletal development.[19,56] However, as only pathogenic variants in *HS2ST1* and not *GLCE* (MIM: 612134) have been associated with a human Mendelian disorder to date, the specific requirement of 2-*O*-sulfated IdoA units for human development cannot be determined.

In contrast to GLCE and HS2ST1, the HS 6-*O*-sulfotransferase 1 (HS6ST1 [MIM: 604846]) is one of three 6-*O*-sulfotransferases which adds sulfate to the C6 of *D*-glucosamine units.[1,57] Heterozygous and homozygous missense variants in *HS6ST1* have been shown to contribute, besides other genetic and/or environmental factors, to normosmic isolated gonadotropin-releasing hormone deficiency (IGD) and IGD with an impaired sense of smell (Kallmann syndrome; hypogonadotropic hypogonadism 15 with or without anosmia [MIM: 614880]).[58–61] Some clinical features of IGD or Kallmann syndrome, such as unilateral renal agenesis, cryptorchidism, bone abnormalities, and cleft lip and/or palate (see Balasubramanian and Crowley in GeneReviews in Web Resources), can also be found in individuals with bi-allelic *HS2ST1* variants, further supporting the idea that correctly *O*-sulfated HS is an important modulator of FGF-mediated cell signaling during human development.

Other disorders linked to genes/proteins involved in GAG sulfation are *CHST3*-related skeletal dysplasia (spondyloepiphyseal dysplasia with congenital joint dislocations [MIM: 143095]), Ehlers-Danlos syndrome, musculocontractural type 1 (EDSMC1 [MIM: 601776]), and osteochondrodysplasia, brachydactyly, and overlapping malformed digits (OCBMD [MIM: 618167]).[62,63] *CHST3*-related skeletal dysplasia is typically characterized by short stature, joint dislocations, clubfeet, restricted movement, kyphosis, and minor heart valve dysplasia (see Superti-Furga and Unger in GeneReviews in Web Resources). Bi-allelic variants in *CHST3* encoding carbohydrate sulfotransferase 3 or chondroitin 6-*O*-sulfotransferase 1 lead to functional impairment of the enzyme.[64,65] EDSMC1 is caused by bi-allelic pathogenic variants in *CHST14* that encodes the carbohydrate sulfotransferase 14 (also named dermatan 4-*O*-sulfotransferase 1), catalyzing the 4-*O*-sulfation of GalNAc residues in dermatan sulfate. Clinically the syndrome is characterized by craniofacial dysmorphism, congenital contractures, joint hypermobility, clubfeet, kyphoscoliosis, muscular hypotonia, hyperextensible thin skin, atrial septal defects, and ocular involvement.[66–68] OCBMD has been reported in a Pakistani family with a homozygous in-frame deletion in *CHST11* encoding carbohydrate sulfotransferase 11 (also named chondroitin 4-*O*-sulfotransferase 1).[69] Together, the published and our data show the importance of the GAG sulfation pathway for cartilage and bone development.

In conclusion, our data reveal HS2ST1, an enzyme involved in GAG sulfation, to be associated with a syndromic phenotype comprising neurological, skeletal, and renal abnormalities. Reduced or absent HS 2-*O*-sulfotransferase 1 activity leads to an aberrantly synthesized HS in cells of affected individuals, with a shift in the global sulfation pattern. *HS2ST1* has to be added to a number of other sulfotransferases mutated in skeletal dysplasia and connective tissue disorders.

Data and Code Availability

There are restrictions on the availability of dataset due to data protection reasons.

Supplemental Data

Supplemental Data can be found online at https://doi.org/10.1016/j.ajhg.2020.10.007.

Acknowledgments

The authors declare no competing financial interest. We thank all probands and families for their participation in this study, Inka Jantke and Dennis Zorndt for skillful technical assistance, and the UKE Microscopy Imaging Facility (UMIF) at the University Medical Center Hamburg-Eppendorf for technical support. This work was supported by grants from the Deutsche Forschungsgemeinschaft (KU 1240/6-2 and KU 1240/10-1) and the Federal Ministry of Education and Research (01DQ17003) to K.K., the UK Biotechnology and Biological Sciences Research Council Doctoral Training Programme (BB/J014508/1) to E.B. and C.L.R.M., and the "Praeclare" University of Zurich clinical priority research program grant to A.R.

Declaration of Interests

The authors declare no competing interests.

Received: July 31, 2020
Accepted: October 13, 2020
Published: November 6, 2020

Web Resources

1000 Genomes Project, https://www.internationalgenome.org
Berkeley *Drosophila* Genome Project, https://www.fruitfly.org/seq_tools/splice.html
CADD, https://cadd.gs.washington.edu/
ClinVar, https://www.ncbi.nlm.nih.gov/clinvar/
dbSNP, https://www.ncbi.nlm.nih.gov/projects/SNP
GeneReviews, Balasubramanian, R., and Crowley, W.F., Jr. (1993). Isolated Gonadotropin-Releasing Hormone (GnRH) Deficiency. https://www.ncbi.nlm.nih.gov/books/NBK1334/
GeneReviews, Superti-Furga, A., and Unger, S. (1993). CHST3-Related Skeletal Dysplasia. https://www.ncbi.nlm.nih.gov/books/NBK62112/
gnomAD Browser, https://gnomad.broadinstitute.org
HGMD, http://www.hgmd.cf.ac.uk/ac/index.php
Human Splicing Finder, https://www.genomnis.com/access-hsf
M-CAP, http://bejerano.stanford.edu/MCAP/index.html
NCBI gene, https://www.ncbi.nlm.nih.gov/gene
NetGene2, http://www.cbs.dtu.dk/services/NetGene2/
NHLBI Exome Sequencing Project (ESP), https://evs.gs.washington.edu/EVS/
OMIM, https://www.omim.org
Picard, http://picard.sourceforge.net/
REVEL, https://sites.google.com/site/revelgenomics/
SWISSMODEL, https://swissmodel.expasy.org/

References

1. Esko, J.D., and Lindahl, U. (2001). Molecular diversity of heparan sulfate. J. Clin. Invest. *108*, 169–173.
2. Li, J.P., and Kusche-Gullberg, M. (2016). Heparan Sulfate: Biosynthesis, Structure, and Function. Int. Rev. Cell Mol. Biol. *325*, 215–273.
3. Couchman, J.R. (2010). Transmembrane signaling proteoglycans. Annu. Rev. Cell Dev. Biol. *26*, 89–114.
4. Lin, X. (2004). Functions of heparan sulfate proteoglycans in cell signaling during development. Development *131*, 6009–6021.
5. Lindahl, U., and Li, J.P. (2009). Interactions between heparan sulfate and proteins-design and functional implications. Int. Rev. Cell Mol. Biol. *276*, 105–159.
6. Kreuger, J., Salmivirta, M., Sturiale, L., Giménez-Gallego, G., and Lindahl, U. (2001). Sequence analysis of heparan sulfate epitopes with graded affinities for fibroblast growth factors 1 and 2. J. Biol. Chem. *276*, 30744–30752.
7. Turnbull, J.E., Fernig, D.G., Ke, Y., Wilkinson, M.C., and Gallagher, J.T. (1992). Identification of the basic fibroblast growth factor binding sequence in fibroblast heparan sulfate. J. Biol. Chem. *267*, 10337–10341.
8. Kobayashi, M., Habuchi, H., Yoneda, M., Habuchi, O., and Kimata, K. (1997). Molecular cloning and expression of Chinese hamster ovary cell heparan-sulfate 2-sulfotransferase. J. Biol. Chem. *272*, 13980–13985.
9. Bai, X., and Esko, J.D. (1996). An animal cell mutant defective in heparan sulfate hexuronic acid 2-O-sulfation. J. Biol. Chem. *271*, 17711–17717.
10. Rong, J., Habuchi, H., Kimata, K., Lindahl, U., and Kusche-Gullberg, M. (2001). Substrate specificity of the heparan sulfate hexuronic acid 2-O-sulfotransferase. Biochemistry *40*, 5548–5555.
11. Ledin, J., Staatz, W., Li, J.P., Götte, M., Selleck, S., Kjellén, L., and Spillmann, D. (2004). Heparan sulfate structure in mice with genetically modified heparan sulfate production. J. Biol. Chem. *279*, 42732–42741.
12. Bethea, H.N., Xu, D., Liu, J., and Pedersen, L.C. (2008). Redirecting the substrate specificity of heparan sulfate 2-O-sulfotransferase by structurally guided mutagenesis. Proc. Natl. Acad. Sci. USA *105*, 18724–18729.
13. Xu, D., Song, D., Pedersen, L.C., and Liu, J. (2007). Mutational study of heparan sulfate 2-O-sulfotransferase and chondroitin sulfate 2-O-sulfotransferase. J. Biol. Chem. *282*, 8356–8367.
14. Kamimura, K., Koyama, T., Habuchi, H., Ueda, R., Masu, M., Kimata, K., and Nakato, H. (2006). Specific and flexible roles of heparan sulfate modifications in Drosophila FGF signaling. J. Cell Biol. *174*, 773–778.
15. Kinnunen, T., Huang, Z., Townsend, J., Gatdula, M.M., Brown, J.R., Esko, J.D., and Turnbull, J.E. (2005). Heparan 2-O-sulfotransferase, hst-2, is essential for normal cell migration in Caenorhabditis elegans. Proc. Natl. Acad. Sci. USA *102*, 1507–1512.
16. Bülow, H.E., and Hobert, O. (2004). Differential sulfations and epimerization define heparan sulfate specificity in nervous system development. Neuron *41*, 723–736.
17. Bullock, S.L., Fletcher, J.M., Beddington, R.S., and Wilson, V.A. (1998). Renal agenesis in mice homozygous for a gene trap mutation in the gene encoding heparan sulfate 2-sulfotransferase. Genes Dev. *12*, 1894–1906.
18. Merry, C.L., and Wilson, V.A. (2002). Role of heparan sulfate-2-O-sulfotransferase in the mouse. Biochim. Biophys. Acta *1573*, 319–327.
19. Merry, C.L., Bullock, S.L., Swan, D.C., Backen, A.C., Lyon, M., Beddington, R.S., Wilson, V.A., and Gallagher, J.T. (2001). The molecular phenotype of heparan sulfate in the Hs2st-/- mutant mouse. J. Biol. Chem. *276*, 35429–35434.
20. Li, H., and Durbin, R. (2009). Fast and accurate short read alignment with Burrows-Wheeler transform. Bioinformatics *25*, 1754–1760.
21. McKenna, A., Hanna, M., Banks, E., Sivachenko, A., Cibulskis, K., Kernytsky, A., Garimella, K., Altshuler, D., Gabriel, S., Daly, M., and DePristo, M.A. (2010). The Genome Analysis Toolkit: a MapReduce framework for analyzing next-generation DNA sequencing data. Genome Res. *20*, 1297–1303.
22. Wang, K., Li, M., and Hakonarson, H. (2010). ANNOVAR: functional annotation of genetic variants from high-throughput sequencing data. Nucleic Acids Res. *38*, e164.
23. Harms, F.L., Parthasarathy, P., Zorndt, D., Alawi, M., Fuchs, S., Halliday, B.J., McKeown, C., Sampaio, H., Radhakrishnan, N., Radhakrishnan, S.K., et al. (2020). Biallelic loss-of-function variants in TBC1D2B cause a neurodevelopmental disorder with seizures and gingival overgrowth. Hum. Mutat. https://doi.org/10.1002/humu.24071.
24. Holley, R.J., Deligny, A., Wei, W., Watson, H.A., Niñonuevo, M.R., Dagälv, A., Leary, J.A., Bigger, B.W., Kjellén, L., and Merry, C.L. (2011). Mucopolysaccharidosis type I, unique structure of accumulated heparan sulfate and increased N-sulfotransferase activity in mice lacking α-l-iduronidase. J. Biol. Chem. *286*, 37515–37524.
25. Deakin, J.A., and Lyon, M. (2008). A simplified and sensitive fluorescent method for disaccharide analysis of both heparan sulfate and chondroitin/dermatan sulfates from biological samples. Glycobiology *18*, 483–491.
26. Legerstee, K., Geverts, B., Slotman, J.A., and Houtsmuller, A.B. (2019). Dynamics and distribution of paxillin, vinculin, zyxin

and VASP depend on focal adhesion location and orientation. Sci. Rep. *9*, 10460.
27. Sobreira, N., Schiettecatte, F., Boehm, C., Valle, D., and Hamosh, A. (2015). New tools for Mendelian disease gene identification: PhenoDB variant analysis module; and GeneMatcher, a web-based tool for linking investigators with an interest in the same gene. Hum. Mutat. *36*, 425–431.
28. Karczewski, K.J., Francioli, L.C., Tiao, G., Cummings, B.B., Alföldi, J., Wang, Q., Collins, R.L., Laricchia, K.M., Ganna, A., Birnbaum, D.P., et al.; Genome Aggregation Database Consortium (2020). The mutational constraint spectrum quantified from variation in 141,456 humans. Nature *581*, 434–443.
29. Harmer, N.J. (2006). Insights into the role of heparan sulphate in fibroblast growth factor signalling. Biochem. Soc. Trans. *34*, 442–445.
30. Mohammadi, M., Olsen, S.K., and Ibrahimi, O.A. (2005). Structural basis for fibroblast growth factor receptor activation. Cytokine Growth Factor Rev. *16*, 107–137.
31. Delehedde, M., Lyon, M., Gallagher, J.T., Rudland, P.S., and Fernig, D.G. (2002). Fibroblast growth factor-2 binds to small heparin-derived oligosaccharides and stimulates a sustained phosphorylation of p42/44 mitogen-activated protein kinase and proliferation of rat mammary fibroblasts. Biochem. J. *366*, 235–244.
32. Jastrebova, N., Vanwildemeersch, M., Lindahl, U., and Spillmann, D. (2010). Heparan sulfate domain organization and sulfation modulate FGF-induced cell signaling. J. Biol. Chem. *285*, 26842–26851.
33. Casale, J., and Crane, J.S. (2020) (Treasure Island, FL: Biochemistry, Glycosaminoglycans. In StatPearls).
34. Delehedde, M., Seve, M., Sergeant, N., Wartelle, I., Lyon, M., Rudland, P.S., and Fernig, D.G. (2000). Fibroblast growth factor-2 stimulation of p42/44MAPK phosphorylation and IkappaB degradation is regulated by heparan sulfate/heparin in rat mammary fibroblasts. J. Biol. Chem. *275*, 33905–33910.
35. Taylor, K.R., Rudisill, J.A., and Gallo, R.L. (2005). Structural and sequence motifs in dermatan sulfate for promoting fibroblast growth factor-2 (FGF-2) and FGF-7 activity. J. Biol. Chem. *280*, 5300–5306.
36. Pellegrini, L., Burke, D.F., von Delft, F., Mulloy, B., and Blundell, T.L. (2000). Crystal structure of fibroblast growth factor receptor ectodomain bound to ligand and heparin. Nature *407*, 1029–1034.
37. Horowitz, A., Tkachenko, E., and Simons, M. (2002). Fibroblast growth factor-specific modulation of cellular response by syndecan-4. J. Cell Biol. *157*, 715–725.
38. Rieck, P.W., Cholidis, S., and Hartmann, C. (2001). Intracellular signaling pathway of FGF-2-modulated corneal endothelial cell migration during wound healing in vitro. Exp. Eye Res. *73*, 639–650.
39. Woods, A., and Couchman, J.R. (1992). Heparan sulfate proteoglycans and signalling in cell adhesion. Adv. Exp. Med. Biol. *313*, 87–96.
40. Brown, M.C., and Turner, C.E. (2004). Paxillin: adapting to change. Physiol. Rev. *84*, 1315–1339.
41. Webb, D.J., Brown, C.M., and Horwitz, A.F. (2003). Illuminating adhesion complexes in migrating cells: moving toward a bright future. Curr. Opin. Cell Biol. *15*, 614–620.
42. Bruyère, J., Roy, E., Ausseil, J., Lemonnier, T., Teyre, G., Bohl, D., Etienne-Manneville, S., Lortat-Jacob, H., Heard, J.M., and Vitry, S. (2015). Heparan sulfate saccharides modify focal adhesions: implication in mucopolysaccharidosis neuropathophysiology. J. Mol. Biol. *427*, 775–791.
43. Mahalingam, Y., Gallagher, J.T., and Couchman, J.R. (2007). Cellular adhesion responses to the heparin-binding (HepII) domain of fibronectin require heparan sulfate with specific properties. J. Biol. Chem. *282*, 3221–3230.
44. Nikolovska, K., Spillmann, D., and Seidler, D.G. (2015). Uronyl 2-O sulfotransferase potentiates Fgf2-induced cell migration. J. Cell Sci. *128*, 460–471.
45. Liu, C., Sheng, J., Krahn, J.M., Perera, L., Xu, Y., Hsieh, P.H., Dou, W., Liu, J., and Pedersen, L.C. (2014). Molecular mechanism of substrate specificity for heparan sulfate 2-O-sulfotransferase. J. Biol. Chem. *289*, 13407–13418.
46. Okina, E., Grossi, A., Gopal, S., Multhaupt, H.A., and Couchman, J.R. (2012). Alpha-actinin interactions with syndecan-4 are integral to fibroblast-matrix adhesion and regulate cytoskeletal architecture. Int. J. Biochem. Cell Biol. *44*, 2161–2174.
47. Bartolini, B., Thelin, M.A., Svensson, L., Ghiselli, G., van Kuppevelt, T.H., Malmström, A., and Maccarana, M. (2013). Iduronic acid in chondroitin/dermatan sulfate affects directional migration of aortic smooth muscle cells. PLoS ONE *8*, e66704.
48. Malmström, A., Bartolini, B., Thelin, M.A., Pacheco, B., and Maccarana, M. (2012). Iduronic acid in chondroitin/dermatan sulfate: biosynthesis and biological function. J. Histochem. Cytochem. *60*, 916–925.
49. Tillo, M., Charoy, C., Schwarz, Q., Maden, C.H., Davidson, K., Fantin, A., and Ruhrberg, C. (2016). 2- and 6-O-sulfated proteoglycans have distinct and complementary roles in cranial axon guidance and motor neuron migration. Development *143*, 1907–1913.
50. Shah, M.M., Sakurai, H., Gallegos, T.F., Sweeney, D.E., Bush, K.T., Esko, J.D., and Nigam, S.K. (2011). Growth factor-dependent branching of the ureteric bud is modulated by selective 6-O sulfation of heparan sulfate. Dev. Biol. *356*, 19–27.
51. Shah, M.M., Tee, J.B., Meyer, T., Meyer-Schwesinger, C., Choi, Y., Sweeney, D.E., Gallegos, T.F., Johkura, K., Rosines, E., Kouznetsova, V., et al. (2009). The instructive role of metanephric mesenchyme in ureteric bud patterning, sculpting, and maturation and its potential ability to buffer ureteric bud branching defects. Am. J. Physiol. Renal Physiol. *297*, F1330–F1341.
52. Kobayashi, T., Habuchi, H., Tamura, K., Ide, H., and Kimata, K. (2007). Essential role of heparan sulfate 2-O-sulfotransferase in chick limb bud patterning and development. J. Biol. Chem. *282*, 19589–19597.
53. Conway, C.D., Howe, K.M., Nettleton, N.K., Price, D.J., Mason, J.O., and Pratt, T. (2011). Heparan sulfate sugar modifications mediate the functions of slits and other factors needed for mouse forebrain commissure development. J. Neurosci. *31*, 1955–1970.
54. Clegg, J.M., Parkin, H.M., Mason, J.O., and Pratt, T. (2019). Heparan Sulfate Sulfation by Hs2st Restricts Astroglial Precursor Somal Translocation in Developing Mouse Forebrain by a Non-Cell-Autonomous Mechanism. J. Neurosci. *39*, 1386–1404.
55. Clegg, J.M., Conway, C.D., Howe, K.M., Price, D.J., Mason, J.O., Turnbull, J.E., Basson, M.A., and Pratt, T. (2014). Heparan sulfotransferases Hs6st1 and Hs2st keep Erk in check for mouse corpus callosum development. J. Neurosci. *34*, 2389–2401.
56. Li, J.P., Gong, F., Hagner-McWhirter, A., Forsberg, E., Abrink, M., Kisilevsky, R., Zhang, X., and Lindahl, U. (2003). Targeted disruption of a murine glucuronyl C5-epimerase gene results

in heparan sulfate lacking L-iduronic acid and in neonatal lethality. J. Biol. Chem. *278*, 28363–28366.

57. Habuchi, H., Tanaka, M., Habuchi, O., Yoshida, K., Suzuki, H., Ban, K., and Kimata, K. (2000). The occurrence of three isoforms of heparan sulfate 6-O-sulfotransferase having different specificities for hexuronic acid adjacent to the targeted N-sulfoglucosamine. J. Biol. Chem. *275*, 2859–2868.
58. Tornberg, J., Sykiotis, G.P., Keefe, K., Plummer, L., Hoang, X., Hall, J.E., Quinton, R., Seminara, S.B., Hughes, V., Van Vliet, G., et al. (2011). Heparan sulfate 6-O-sulfotransferase 1, a gene involved in extracellular sugar modifications, is mutated in patients with idiopathic hypogonadotrophic hypogonadism. Proc. Natl. Acad. Sci. USA *108*, 11524–11529.
59. Miraoui, H., Dwyer, A.A., Sykiotis, G.P., Plummer, L., Chung, W., Feng, B., Beenken, A., Clarke, J., Pers, T.H., Dworzynski, P., et al. (2013). Mutations in FGF17, IL17RD, DUSP6, SPRY4, and FLRT3 are identified in individuals with congenital hypogonadotropic hypogonadism. Am. J. Hum. Genet. *92*, 725–743.
60. Falardeau, J., Chung, W.C., Beenken, A., Raivio, T., Plummer, L., Sidis, Y., Jacobson-Dickman, E.E., Eliseenkova, A.V., Ma, J., Dwyer, A., et al. (2008). Decreased FGF8 signaling causes deficiency of gonadotropin-releasing hormone in humans and mice. J. Clin. Invest. *118*, 2822–2831.
61. Dodé, C., Levilliers, J., Dupont, J.M., De Paepe, A., Le Dû, N., Soussi-Yanicostas, N., Coimbra, R.S., Delmaghani, S., Compain-Nouaille, S., Baverel, F., et al. (2003). Loss-of-function mutations in FGFR1 cause autosomal dominant Kallmann syndrome. Nat. Genet. *33*, 463–465.
62. Paganini, C., Gramegna Tota, C., Superti-Furga, A., and Rossi, A. (2020). Skeletal Dysplasias Caused by Sulfation Defects. Int. J. Mol. Sci. *21*, 21.
63. Paganini, C., Costantini, R., Superti-Furga, A., and Rossi, A. (2019). Bone and connective tissue disorders caused by defects in glycosaminoglycan biosynthesis: a panoramic view. FEBS J. *286*, 3008–3032.
64. Hermanns, P., Unger, S., Rossi, A., Perez-Aytes, A., Cortina, H., Bonafé, L., Boccone, L., Setzu, V., Dutoit, M., Sangiorgi, L., et al. (2008). Congenital joint dislocations caused by carbohydrate sulfotransferase 3 deficiency in recessive Larsen syndrome and humero-spinal dysostosis. Am. J. Hum. Genet. *82*, 1368–1374.
65. Thiele, H., Sakano, M., Kitagawa, H., Sugahara, K., Rajab, A., Höhne, W., Ritter, H., Leschik, G., Nürnberg, P., and Mundlos, S. (2004). Loss of chondroitin 6-O-sulfotransferase-1 function results in severe human chondrodysplasia with progressive spinal involvement. Proc. Natl. Acad. Sci. USA *101*, 10155–10160.
66. Dündar, M., Müller, T., Zhang, Q., Pan, J., Steinmann, B., Vodopiutz, J., Gruber, R., Sonoda, T., Krabichler, B., Utermann, G., et al. (2009). Loss of dermatan-4-sulfotransferase 1 function results in adducted thumb-clubfoot syndrome. Am. J. Hum. Genet. *85*, 873–882.
67. Malfait, F., Syx, D., Vlummens, P., Symoens, S., Nampoothiri, S., Hermanns-Lê, T., Van Laer, L., and De Paepe, A. (2010). Musculocontractural Ehlers-Danlos Syndrome (former EDS type VIB) and adducted thumb clubfoot syndrome (ATCS) represent a single clinical entity caused by mutations in the dermatan-4-sulfotransferase 1 encoding CHST14 gene. Hum. Mutat. *31*, 1233–1239.
68. Miyake, N., Kosho, T., Mizumoto, S., Furuichi, T., Hatamochi, A., Nagashima, Y., Arai, E., Takahashi, K., Kawamura, R., Wakui, K., et al. (2010). Loss-of-function mutations of CHST14 in a new type of Ehlers-Danlos syndrome. Hum. Mutat. *31*, 966–974.
69. Shabbir, R.M.K., Nalbant, G., Ahmad, N., Malik, S., and Tolun, A. (2018). Homozygous *CHST11* mutation in chondrodysplasia, brachydactyly, overriding digits, clino-symphalangism and synpolydactyly. J. Med. Genet. *55*, 489–496.